THE EFFECT OF DOWNSTREAM PROCESSING STEPS ON PROCESS YIELD AND PROTEIN QUALITY

A Thesis

by

EMMA ROSE FOSTER

Submitted to the Graduate and Professional School of
Texas A&M University
in partial fulfillment of the requirements for the degree of

MASTER OF SCIENCE

Chair of Committee,	Zivko Nikolov
Committee Members,	Sandun Fernando
	Katy Kao
	Maria King
Head of Department,	Patricia Smith

May 2023

Major Subject: Biological and Agricultural Engineering

ABSTRACT

Proteinaceous drug substances produced in or recovered from a biological source are called biologics or biopharmaceuticals. This class of drugs has grown exponentially with the advances made in genetic engineering and recombinant DNA technology in the 1970s and 80s. Many previously untreatable conditions and autoimmune diseases now have treatment options thanks to biologics produced by genetically modified mammalian cell cultures. These proteinaceous therapies are often large subunit or multi-subunit substances requiring specific folding mechanisms to take place for an active version of the product. Mammalian cell machinery allows for proper post-translational modification and folding.

The biologics industry brings in an annual $275 billion in revenue and more than a quarter of all FDA approved drugs are in this category. Biologics are more complex drug substances than the traditional small-molecule drugs produced by chemical synthesis and their cost of manufacture follows suit: biologics range from $100- 1000/g while synthesized drugs can be made as cheaply as $5/g. The high cost is reflected in the finely-tuned growth media and operating parameter control required for cultivation, and the optimized multi-step purification scheme. The steep cost to manufacture necessitates high yield purification steps for economic feasibility.

Careful consideration for each purification step is required to meet high recovery demands. Investigation of buffer chases after depth filtration for primary clarification with mAb producing CHO cultures brought insight to host cell protein and dsDNA removal as well as mAb recovery. While performing a high ionic strength buffer chase could recover more mAb, the tradeoff of dsDNA released was unfavorable.

Affinity purification of two COVID-19 spike protein variants (S-2P and HexaPro) produced in HEK 293 cell cultures was also investigated. The spike variants were designed with cleavable purification tags enabling affinity purification and subsequent tag removal. While investigating various desalting steps (gel filtration, normal flow filtration with spin tubes, and TFF) of affinity purified spike proteins a visible turbidity was observed in TFF-processed samples. The presence of turbidity (presumably due to protein aggregation) prompted further investigation of the origin of turbidity. Performing SEC on affinity purified spike protein samples confirmed the presence of spike protein aggregates. Once tags were cleaved from the sample, SEC analysis estimated the trimeric spike protein primarily in the non-aggregated form and concluded that the very hydrophobic nature of the amino acid residues that make up the tails encouraged aggregation of the trimers in an aqueous environment.

DEDICATION

To my beloved mother, father, brother, and grandmother for their never-ending support and encouragement.

ACKNOWLEDGEMENTS

I would like to thank my committee chair, Dr. Zivko Nikolov, for his support, faith in me, and flexibility throughout my graduate studies. I would also like to thank my committee members, Dr. Sandun Fernando, Dr. Maria King, and Dr. Katy Kao, and departmental faculty and staff for their support and flexibility throughout the course of my degree.

A big thanks go to my colleagues, Dr. Ayswarya Ravi and Dr. Laura Soto Sierra, of the Bioseparations Lab for their mentorship both in and out of the lab; they were invaluable to my laboratory training and their friendship made it such an enjoyable place to work. Thank you to the researchers at the National Center for Therapeutics Manufacturing for their expertise, sharing their facility and equipment, and promoting a collaborative research space.

Finally, thank you to my mother for her daily phone calls, reassurance, and love; my father for supporting me no matter the circumstance; my brother for making many trips to visit; and my whole family for their persistence in getting me the help I needed to achieve this milestone.

CONTRIBUTORS AND FUNDING SOURCES

Contributors

This work was supervised by a thesis committee consisting of Professors Dr. Zivko Nikolov [advisor], Dr. Sandun Fernando, and Dr. Maria King of the Department of Biological and Agricultural Engineering and Professor Dr. Katy Kao of the Department of Chemical Engineering.

Experimentation conducted for Chapter 2 was supervised and assisted by Dr. Ayswarya Ravi. The collaborators who provided the cell culture stocks utilized in Chapter 3 were Dr. Jimmy Gollihar and Dr. Jason McLelland of the Army Research Lab – South. The analyses depicted in Figures 19, 20, and 21 were conducted in part by researchers at the National Center for Therapeutics Manufacturing.

All other work conducted for the thesis was completed by the student independently.

Funding Sources

Graduate study was supported by assistantship from Dr. Nikolov and the Biological and Agricultural Engineering Department at Texas A&M University.

This work was also made possible by the Coronavirus Aid, Relief, and Economic Security (CARES) Act which allotted funding to the National Institute for Innovation in Manufacturing Biopharmaceuticals (NIIMBL); a public-private partnership sponsored by the National Institute of Standards and Technology (NIST) housed in the U.S. Department of Commerce; to support the project “Emergency Production of Covid-19 Spike Protein for Therapeutic Antibodies and Diagnostics.” Its contents are solely the responsibility of the authors and do not necessarily represent the official views of NIIMBL.

NOMENCLATURE

ACE2	angiotensin-converting enzyme 2
BME	2-mercaptoethanol
BSA	bovine serum albumin
CHO	Chinese hamster ovary
CIP	clean-in-place
COVID-19	coronavirus disease 2019
CV	column volume
DI	deionized
dsDNA	double-stranded DNA
DSP	downstream processing
ELISA	enzyme-linked immunosorbent assay
EP	elution pool
HCCS	harvested cell culture supernatant
HCP	host cell protein
HEK 293	human embryonic kidney
HETP	height equivalent to a theoretical plate
HexaPro	spike protein variant with 6 proline substitutions
HPLC	high pressure liquid chromatography
HRV3C	human rhinovirus 3C
IMAC	immobilized metal affinity chromatography
IPA	isopropanol

kDa	kilodalton
LMH	L/m^2h
mAb	monoclonal antibody
MERS	middle east respiratory syndrome
mPES	modified polyethersulfone
MTX	methotrexate
NWP	normalized water permeability
PAGE	polyacrylamide gel electrophoresis
PBS	phosphate buffered saline
pI	Isoelectric point
PTM	Post translation modification
S-2P	spike protein variant with 2 proline substitutions
SARS	severe acute respiratory syndrome
SARS-CoV-2	severe acute respiratory syndrome coronavirus 2
SEC	size-exclusion chromatography
SDS	sodium dodecyl sulfate
SIP	steam-in-place
TMB	3,3′,5,5′-Tetramethylbenzidine
TMP	transmembrane pressure
TFF	tangential flow filtration

TABLE OF CONTENTS

Page

LIST OF FIGURES

Page

LIST OF TABLES

Page

CHAPTER I

INTRODUCTION AND LITERATURE REVIEW

1.1 Introduction

Biologics, also called biotherapies or biopharmaceuticals, are drug substances produced in and/or recovered from a biological source[1]. Recombinant DNA technology advances during the 1970s and 80s allowed the biopharmaceutical sector to grow exponentially thereafter[2]. Current annual revenue from biologics is around $275 billion and more than a quarter of FDA approved drugs are biologics[3]. These new drugs are treating diseases or conditions that have no other treatment options available, but production costs for biologics range from $100-$1000/g whereas traditional chemically synthesized drugs can be manufactured for less than $5/g[4]. These high drug costs may be diminished by insurance or government assistance, but the high prices are still passed along to the patient, either making the life-saving treatments inaccessible or pushing patients into medical debt. It is paramount for the industry to continue process development aimed at reducing costs of biotherapeutics while providing the same safe, high-quality product.

1.1.1 Expression platforms

The FDA regulates both the expression system as well as the biotherapies produced by them. The most used bacterial expression platform is *Escherichia coli* and the most commonly used mammalian expression platform is Chinese Hamster Ovary (CHO) cells[5]. The expression platform is chosen based on the needs of the therapeutic protein. Bacterial expression systems (1) are easily genetically modified, (2) have fast growth rates, (3) can provide high titers of small,

single-domain proteins or protein fragments, and achieve all of this for (4) relatively low cost[6]. However, they are incapable of mammalian-like post translation modification (PTM). Most native proteins produced in prokaryotes are single-domain while roughly 70% of native eukaryotic proteins are multi-domain. As such, prokaryotic chaperonins operate quite differently than eukaryotic chaperonins and are unable to reliably fold complex, multi-subunit proteins[7]. For this reason, mammalian expression platforms are the more attractive option for larger, multi-unit proteins and/or those requiring mammalian PTMs. Limitations of utilizing a mammalian expression system are tied to the cost of cultivation. Mammalian cell cultures require finely tuned media components, more expensive bioreactors, and tighter operating parameter control all adding to the bottom line. Traditionally, mammalian expression platforms achieved lower starting titers than bacterial expression platforms though much improvement has been made in this area in recent years to increase recombinant protein production in mammalian cell cultures[8]. The choice of expression system is a balance between the complexity of the target molecule and the cost of its cultivation.

1.1.2 Downstream processing design

Each therapeutic protein is a unique molecule with a distinct size, charge, and hydrophobicity that necessitates a customized downstream processing (DSP) scheme. The physiochemical properties of the therapeutic protein must be investigated and exploited to partition the product away from the cellular impurities[9]. To achieve a highly pure (99.9%) drug substance, unit operations are chosen based on the expression system, the location of the product (intracellularly – cytoplasmic or periplasmic, extracellularly, etc), the stability of the product,

and the impurities derived from cultivation such as host cell protein (HCP) and impurities from the culture media[10].

The overall quality of the therapeutic is dictated by its manufacturing process[4], but there is no standardized sequence of unit operations to purify therapeutic proteins. All biopharmaceutical purification trains will have three to four key phases: Primary Recovery, Isolation (could include concentration and stabilization as separate or combined steps), Purification, and Polishing[10]. Downstream process development is governed by heuristics ("rules-of-thumb") as a starting point for screening experiments[10, 11]. The purification scheme must be rationally chosen and optimized iteratively as each additional manufacturing step requires large capital investment and validation costs to ensure sterility and performance[10]. For this reason, DSP typically becomes the bottleneck of the process scheme and accounts for 50-80% of manufacturing costs[10]. The goal of DSP is to create the shortest string of unit operations that achieves the highest product purity as shown in ***Figure 1***.

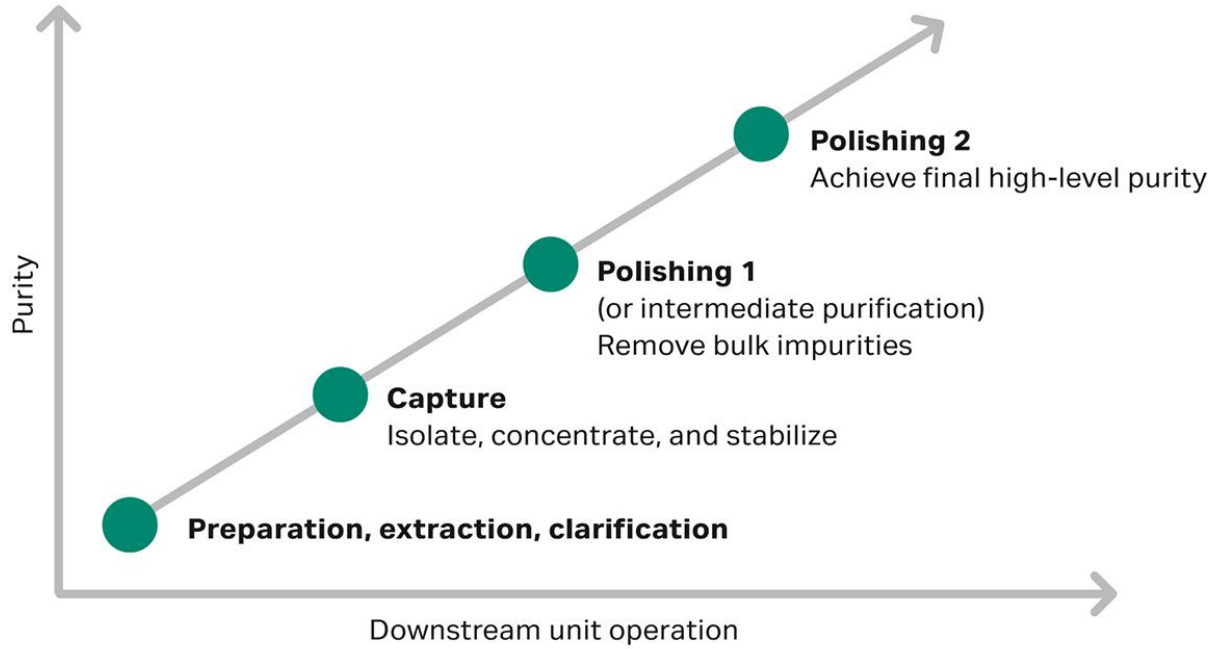

Figure 1 Graphical representation of purity increase as DSP steps are coupled © Copyright Cytiva – Reproduced with permission from Cytiva [12]

1.1.2.1 Harvest and clarification

As starting titers from mammalian cell cultures have substantially increased over the past decade, the associated HCP and process-related impurities have also increased[13] straining the downstream purification process[14, 15]. The primary recovery step, also called the "harvest", is the initial step of downstream processing and is the separation of the solid and liquid products after the production culture is terminated[16]. This step is completely dependent upon the location of the recombinant protein. Intracellularly produced proteins will utilize a harvest step that retains the biomass whereas secreted proteins will have a harvest step that discards the cells[16]. A comparison of the harvest procedures between an extracellularly and intracellularly produced protein are shown in ***Figure 2***.

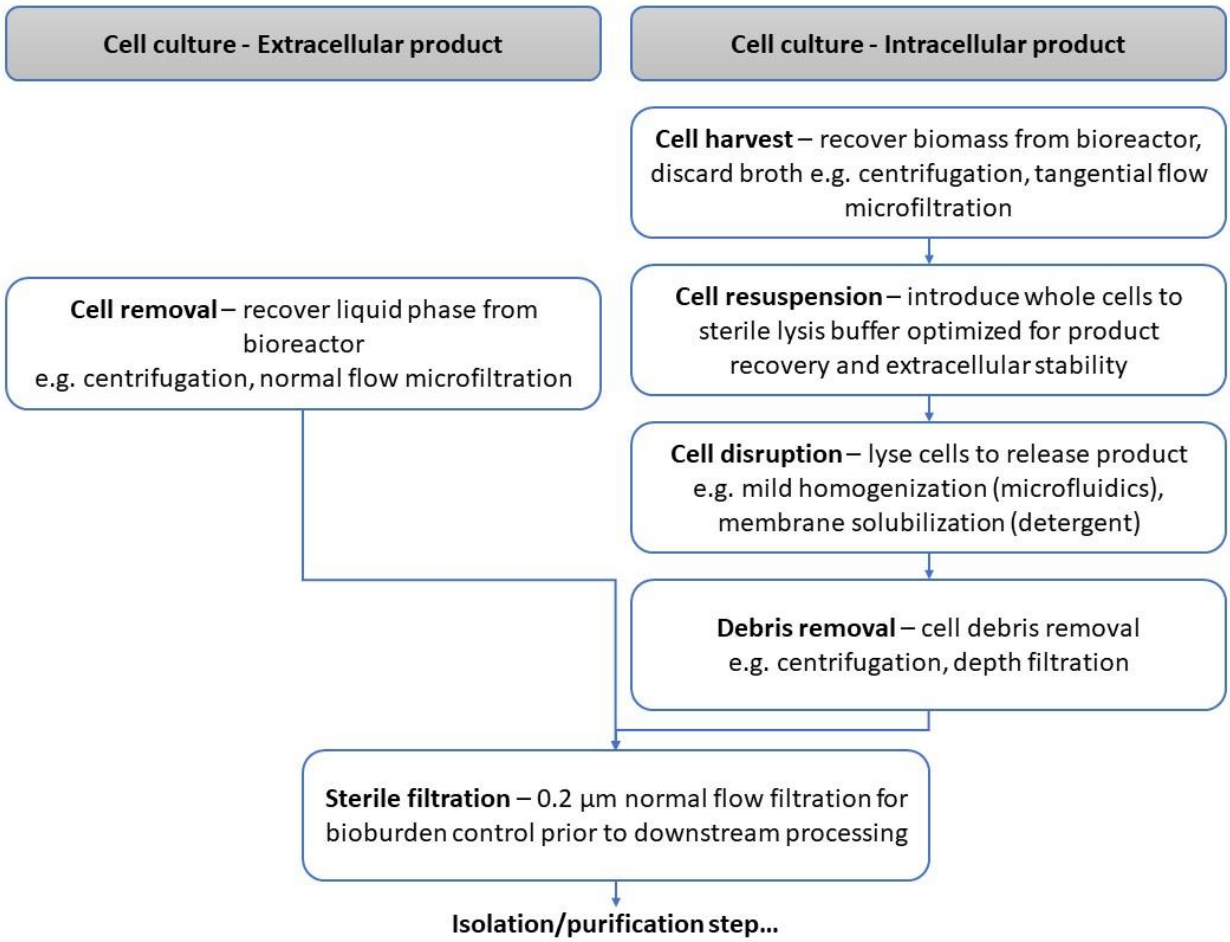

Figure 2 Flowchart comparing harvest processing steps between extracellularly and intracellularly produced protein from a mammalian cell culture

A paramount step before further downstream processing is clarification of the harvested material. Clarification refers to the removal of any remaining whole cells, cell debris, or particulate matter from the processing stream[17] and is generally achieved through 0.2 µm normal flow microfiltration although a tangential flow microfiltration clarification step can be utilized with secreted protein.

Tangential flow microfiltration is an option for extracellular products to recover the biologic as it permeates the membrane while whole cells are retained[18, 19]. If the membrane pore size selected is small enough, the resulting permeate requires little further filtration. But

TFF comes with limitations; as pore size is decreased, membrane fouling and pore plugging are more likely to occur as concentration of the cell culture proceeds[18]. Mammalian cell cultivation techniques have advanced remarkably for secretory protein production and often involve harvesting cultures at viability levels <50%. The tradeoff for increased product yield at these viability readings include greater cell debris and colloidal content profile present in the harvested culture broth[20]. These additional impurities contribute to membrane fouling and pore plugging and so, TFF is not suited as a clarification step when solids content are ≥3%; the case for nearly all mammalian production cultures[19].

Recent discoveries have been made regarding the adsorptive properties of depth filter media[21]. Specifically, depth filter media has been shown to adsorb soluble impurities like HCP and DNA while also performing the designated task of sterile filtration[14, 22]. In an additional study, synthetic filter media was shown to robustly reduce HCP during clarification of mAb products even when media components were altered[22].

1.1.2.2 Product isolation with affinity chromatography

The objective of product isolation is to remove many impurities away from the product and reduce the volume of clarified feed – either cell culture supernatant or *E. coli* lysate. Because of this, the first step in protein recovery is often referred to as the "capture" step. The capture step of therapeutic proteins is typically performed by adsorption-type chromatography and can be classified as a solute-solute separation method[16]. A powerful adsorption chromatography method for target protein molecule isolation is affinity chromatography. Affinity resins all exploit biological binding interactions to capture the target molecule within the stationary phase while impurities flow through the column. Elution of the target molecule differs depending on

the affinity resin selected and can be achieved by altering the pH, ionic strength, or introducing a displacement molecule with a higher affinity for the ligand than the target molecule, replacing it on the stationary phase. With proper optimization, a single affinity chromatography step gives a substantial purification-fold increase[16].

There are relatively few affinity chromatography resins on the market today utilized in manufacturing. Protein A resins utilize an immobilized protein A originally found in the cell wall of *Staphylococcus aureus*[16]. Protein A has a specific binding affinity for the Fc portion (***Figure 3***) of antibodies[23]. Monoclonal antibody (mAb) manufacturing is one of the only therapeutics with a distinct downstream processing template and the primary capture step is almost always Protein A affinity chromatography[14]. Since the Fc domain is a naturally occurring protein sequence in mammalian cells, Fc-fusion proteins are allowable in pharmaceuticals as well as diagnostics. A limitation of protein A chromatography is the high cost of resin media; as much as $12,000/L[23]. Additionally, protein A chromatography is limited by the sensitivity of the protein A ligand and the column's binding capacity can be affected by nonspecific binding of HCP[21]. Elution from the protein A column is achieved by lowering pH that could lead to precipitation of HCP impurities and aggregation of mAbs. Precipitated HCP that remain on the stationary phase may clog the column matrix and decrease the efficacy of resin regeneration[21]. For this reason, care should be taken to reduce HCP loading on the capture step, and this can be achieved with optimized depth filtration.

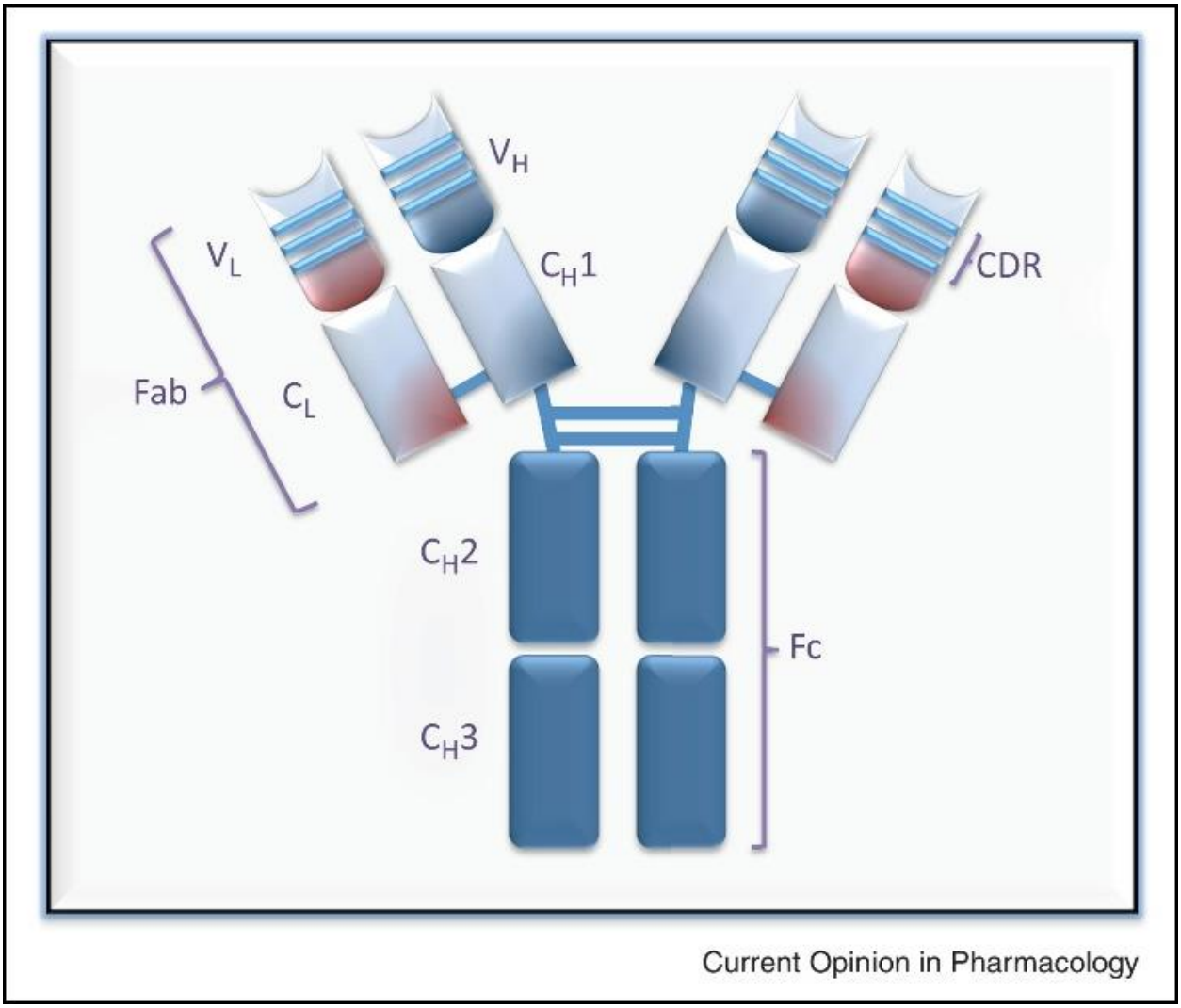

Figure 3 Diagram of a monoclonal antibody structure with the Fc region labeled – Reproduced with permission from [24]

Another affinity option is Immobilized Metal Affinity Chromatography (IMAC), which exploits the interactions between transition metals and the amino acid sequence of the target protein. Transition metals like copper, nickel, and cobalt have an inherent affinity towards histidine residues diagramed in ***Figure 4***. A His-tag, a string of 6-9 histidine amino acids in a row, can be added to either end of a recombinant protein for easy purification. IMAC resin can either come pre-charged with a metal ion strongly bound to the media or uncharged allowing the researcher to immobilize the metal ion of their choosing through ionic interactions. While IMAC

can increase the purification fold of the target product, limitations of IMAC exist. His-tagged proteins are not allowed in drug products, so this purification method is only utilized for diagnostic products and pre-clinical trial applications of biotherapeutic molecules. Knowledge of the cell culture media components is paramount because any chelating agent will affect the bond between the metal ion and the ligand. If a replacer, such as imidazole, is utilized for elution, it is introduced into the processing stream and requires subsequent removal[16].

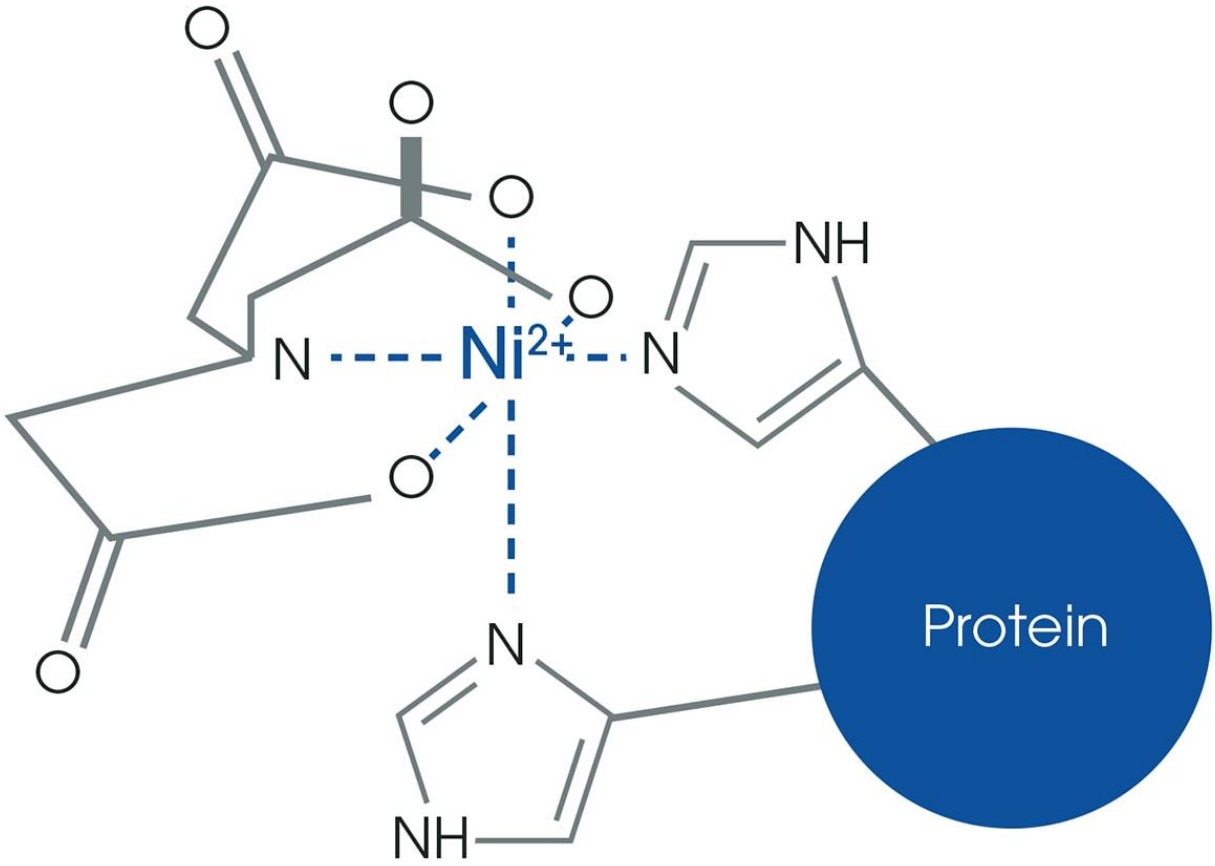

Figure 4 His-Tag protein bound to Nickel charged IMAC resin © Copyright abcam – Reproduced with permission from [25]

1.1.2.3 Purification

Beyond the initial capture step, additional purification unit operations are required to achieve a highly pure, pharmaceutical-grade target molecule. Impurities that remain in the

process stream at this stage share similar biochemical properties to the target molecule - they might have co-eluted with the protein of interest during the capture step or could be truncated or aggregated forms of the target molecule[16]. To separate these similar chemistry species, different resin chemistry and process conditions (pH, conductivity) are typically required. For example, after an affinity chromatography capture step the most common solute-solute separation methods used are ion exchange, hydrophobic interaction, and mixed modal chromatography. The selection of best purification resin is governed by differential chemical properties (mainly hydrophobicity and pI) between residual impurities and the target protein.

1.1.2.4 Polishing

The last downstream processing step that follows a purification step is referred to as polishing. Two methods commonly used as polishing steps in protein purification trains are size exclusion chromatography (SEC) and tangential flow filtration (TFF).

Size exclusion chromatography (SEC) can be an attractive option during this stage of downstream processing. SEC does not employ adsorptive mechanisms to achieve separation. Instead, solutes are slowed as they pass into and around the pores of the resin matrix. Molecules that are larger than the largest pore size are excluded entirely, and they pass through the packed bed first. This is referred to as the exclusion limit and is a characteristic of the SEC medium. Smaller molecules get caught up in the pores of the resin and are effectively retarded. The smallest solutes have the most options of pores to enter and so their flow path through the column is lengthened, rendering them the last species to exit the column[16].

Separation between the truncated, aggregated, and therapeutic forms of the target molecule, and any additional impurities of differing sizes can be achieved with a finely tuned

SEC purification step. Limitations of SEC include the separation range and loading capacity of the column. If the species to be separated are not clearly resolved then either different operating parameters or resin media are needed[26]. Because SEC depends entirely upon the solutes path through the packed bed and not on adsorptive properties, the loading capacity for SEC resin media remains low and is therefore expensive as larger and larger columns are required for large loads. For this reason, SEC is usually one of the final purification strategies employed so that the smallest, and therefore cheapest, column can be utilized to reduce cost[16].

Tangential flow filtration (TFF), also called crossflow filtration, is the workhorse of biopharmaceutical downstream processing. The TFF system can be used in ultrafiltration mode for product concentration (water removal/separation from target protein) or in diafiltration mode for buffer exchange (pH adjustment) and desalting (ionic strength adjustment).

During TFF concentration, the process stream is pumped parallel to the membrane surface. The membrane pore size must be carefully selected to retain the solute of interest on the "top" side of the membrane while the liquid phase and any smaller sized species are able to freely permeate the membrane pores and out of the process stream. During this pumping process, the solute concentration of the retentate increases as a direct result of the decreased process volume.

An additional attribute of TFF is diafiltration, a process similar to dialysis. Instead of the process volume decreasing, a constant process volume is maintained by the addition of fresh buffer introduced to the processing stream at the same rate the permeate is leaving the processing stream. The result is a constant working volume that is slowly transitioned from its initial buffering conditions to the new buffering conditions[16]. Diafiltration is utilized for nearly all

biologics as it is paramount that the recombinant protein is introduced to buffering conditions that improve stability of the bulk drug substance[16, 27].

Injectable protein products must be highly concentrated to reduce the dosing volume, packaging requirements, transportation costs, and overall discomfort for the patient[28]. Achieving highly concentrated protein products could be challenging due to increased process stream viscosity and the risk of product aggregation. For example, concentrations greater than 100 mg/mL are needed to administer therapeutic antibodies in a single, 1-2 mL injection for the patient[28]. Limitations of ultrafiltration and diafiltration are related to the dynamic nature of the unit operation and must be carefully considered when designing the downstream processing train[27]. At high protein concentrations, permeate flux is decreased due to the viscosity of the solution as well as the osmotic pressure required to continue driving liquid across the membrane[29]. Additionally, the shear stresses experienced by the protein as the process stream is pumped through the TFF equipment can break delicate proteins apart, induce protein aggregation, or both[27].

1.1.3 Therapeutic protein aggregation

Of meaningful concern during downstream processing design is the formation of aggregates which is possible throughout all stages of product handling: during subsequent manufacturing steps, storage and shipment, and possibly even during drug delivery[30, 31]. Aggregated therapeutic protein can elicit a strong immune reaction *in vivo*; an ideal response for vaccines but a grave concern for drug therapies. If the body attacks the drug product thinking it is an antigen, the drug can be rendered ineffective for the patient[31, 32]. Many protein therapeutics target chronic diseases with few alternative treatment options so drug tolerance can

become life-threatening for the patient[31]. Buffering conditions play a pivotal role in aqueous protein stability; either inducing or mitigating aggregation dynamics of the therapeutic but these buffer components must also not affect the activity of the protein product nor cause adverse effects in the patient[33].

1.2 Thesis objectives and organization

The objective of this thesis was to evaluate recombinant protein quality and recovery during downstream processing development by monitoring several factors such as product purity, protein recovery, and aggregation tendencies. After this introductory chapter, the thesis is organized into two main projects as follows:

Chapter 2 “impact of ionic strength of chase buffer after depth filtration on mAb recovery” conveys the findings on the impact of varying ionic strength buffer chases post-harvest (centrifugation) and clarification (depth filtration). It is hypothesized that a higher ionic strength chase buffer will recover more mAb from depth filter.

Chapter 3 “aggregation tendencies of affinity purified spike protein variants” conveys the findings on the influence affinity tags have on the recombinant protein to which they are attached. It was hypothesized that the hydrophobic tails contribute to spike protein agglomeration during downstream processing.

CHAPTER II

IMPACT OF IONIC STRENGTH OF CHASE BUFFER AFTER DEPTH FILTRATION ON MAB RECOVERY

2.1 Introduction

2.1.1 Mammalian cell platforms for mAb production

Monoclonal antibodies (mAbs) are the largest class of therapeutic molecules [34]. Chinese Hamster Ovary (CHO) cells are the preferred expression system for recombinant monoclonal antibodies. They are favored for the ability to perform post translation modifications such as glycosylation, extra-cellular secretion of large molecular weight mAbs in high titer (1-5 g/L) and in high purity [35]. In addition to recombinant mAbs, the typical CHO cell supernatant contains impurities such as host cell proteins (HCPs), DNA, and aggregates that need to be removed to formulate the final therapeutic product [36]. Depth filtration is a popular unit operation for culture clarification; removal of cell debris and to a certain extent the DNA, HCP impurities as well [21].

2.1.2 Clarification

Clarification is a crucial component of harvesting cell cultures producing biopharmaceutical products[20]. The primary objective of clarification is to remove whole cells, cell debris, large particulates, colloidal matter, and any remaining insoluble matter from the clarified cell culture fluid[22]. Removal of particulate and insoluble matter is paramount prior to loading a chromatography column to maintain column efficiency and performance[18]. An increasingly sought after secondary objective of clarification is reducing HCP and DNA from the

processing stream[20]. Many clarification strategies can be employed and coupled during commercial manufacturing[22] and the choice of clarification technique is dependent on upon several factors such as the location of the therapeutic product, harvest volume, and cell viability at time of harvest[20].

2.1.2.1 Centrifugation

Centrifugation is another clarification option though rarely is it used independently[19]. Disk-stack centrifuges are most utilized in industrial settings as they are operated continuously but they also pose the risk of cell lysis due to shear experienced inside the equipment[18, 37]. When production cultures are pushed to viability levels of <50%[20], the dead and dying cells in culture are even more susceptible to shear forces that break them apart and generate cell debris[19, 37]. The centrifuge operating conditions optimized for whole cell settling would be insufficient to remove sheared cell debris and thus a secondary filtration step is necessary[20]. High density cultures also effect centrifugation efficiency[19]. In ***Figure 5*** adapted from Liu et. al[19] and created by Iammarino et. al[38], the nonviable cell density readings of harvested cultures are compared to their resulting centrate turbidity at various feed rate (Q)/equivalent settling area (Sigma) operating conditions. As Q/Sigma increases, centrate quality is greatly reduced[19].

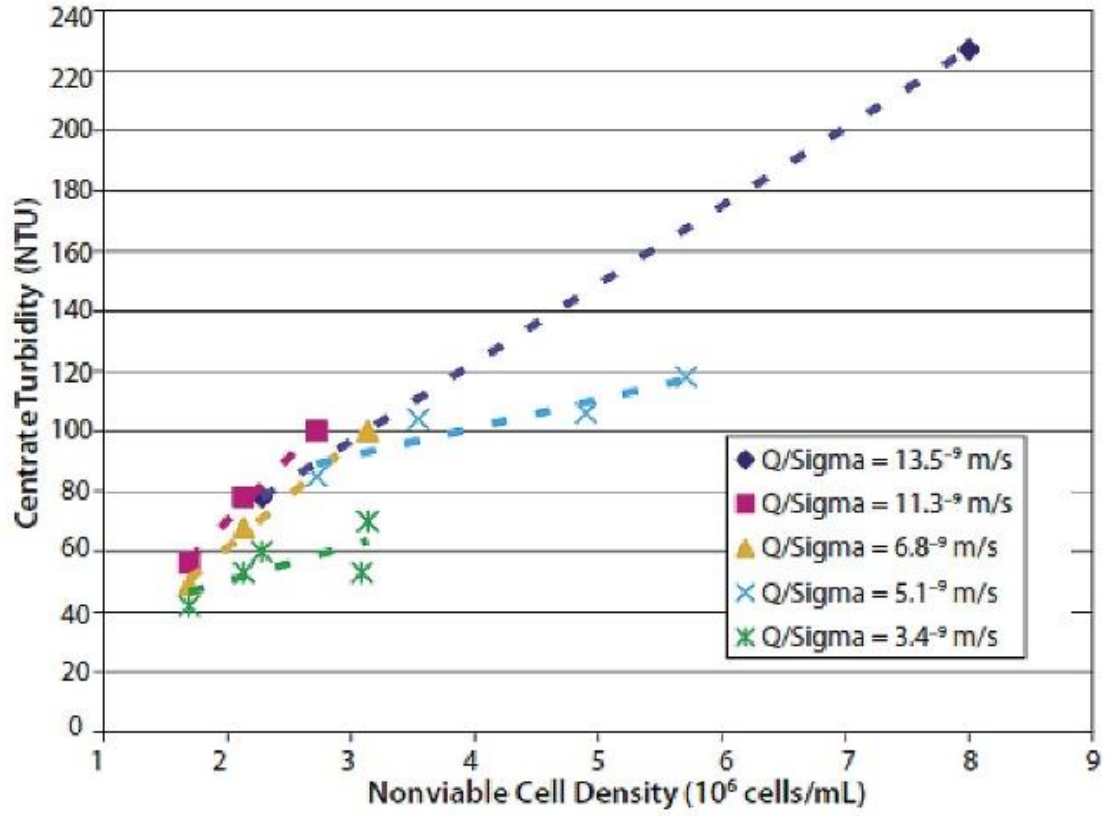

Figure 5 nonviable cell density at time of harvest as it relates to the resulting centrate turbidity – Reproduced with permission from [38]

Disk-stack centrifuges require large capital investment. Technoeconomic analysis was performed by Felo et. al[20] to compare two types of clarification strategies: 1) continuous disk stack centrifugation followed by a single-use depth filtration and 2) multi-stage single-use depth filtration. The analysis showed at bioreactor harvest volumes of <2000L, the two-stage depth filtration clarification process cost was less than the centrifugation and depth filtration process cost. Single-use filters are delivered in sterile packaging ready to be inserted into the production flow path and are disposed of after use bypassing the additional cleaning and validation steps required of centrifuges. This allows the company to reduce equipment downtime due to cleaning as well as utility costs associated with cleaning in place (CIP) and steam in place (SIP) systems [20, 39]. Removing centrifuges from the process exchanges the large capital investment of a

single piece of equipment that requires maintenance and constant validation for small recurring costs of depth filters[39].

2.1.2.2 Depth filtration

Depth filters are already widely used during clarification of cell culture fluid whether on their own or coupled to another harvesting technique. Depth filters are porous beds able to contain particulate matter from the mobile phase within the filter matrix as opposed to excluding large species at the filter's surface[21]. They are comprised of a fibrous bed, a filter aid, a binding polymer that allows the filter material to be formed into sheets, and plastic mesh for reinforcing the internal filter structure[18]. Depth filters have pore-size ratings but do not provide absolute particle clearance in the same way membrane filters do[19]. Filters designed with stepped pore sizes, decreasing as product travels from the top of the filter through the bed to the outlet, show improved turbidity removal from mammalian cell culture[40]. ***Figure 6*** adapted from Shukla (2017) diagrams a cross section of a depth filter and the tortuous path available to the product stream where impurities are removed through mechanical sieving[41].

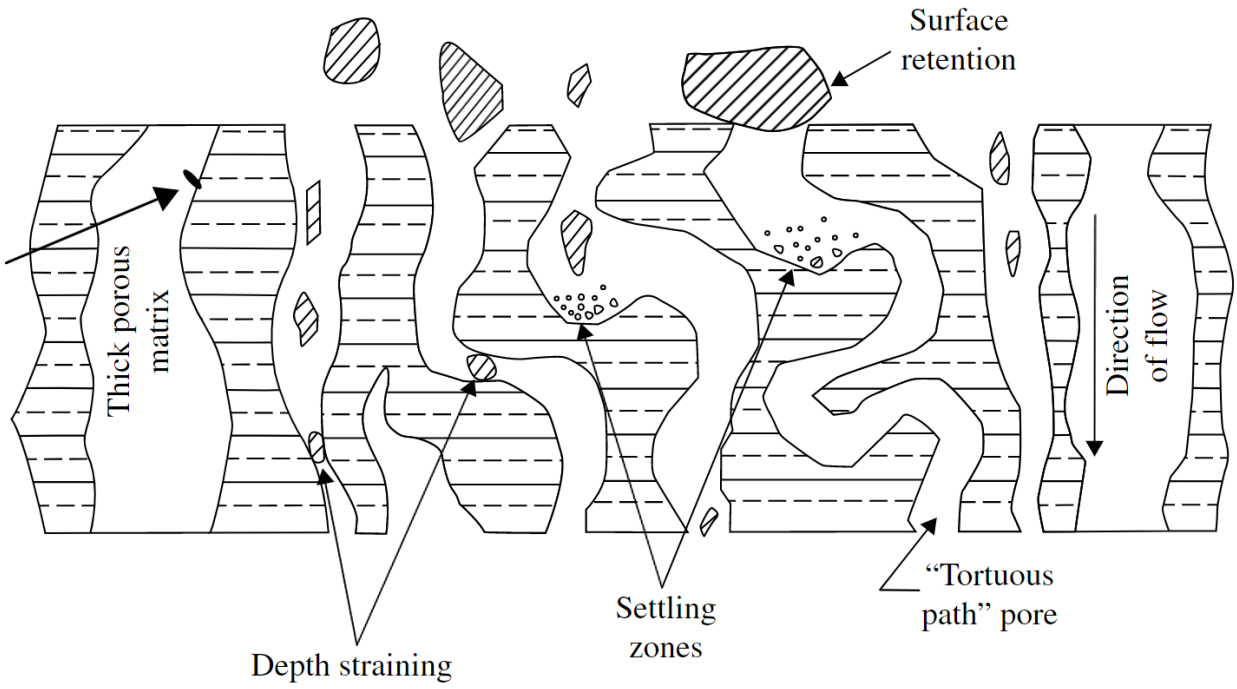

Figure 6 diagram of depth filter's various methods of separation – Reproduced with permission from [42]

Additional separation mechanisms can be employed within a depth filter depending on the properties of the binding polymer utilized in its construction such as electrokinetic adsorption and/or hydrophobic interactions[13, 19]. Positively charged filters have demonstrated endotoxin removal from *E. coli* lysates [18, 19, 21]. Additional studies showed a reduction in DNA content of filtered cell culture fluid which was attributed not only to electrostatic interactions but also hydrophobic interactions between the DNA molecules and the filter media[19, 21]. Using depth filters during clarification of mAb cultures can improve processing quality. Host cell protein is a nuisance during mAb purification on Protein A chromatography columns. Elution from Protein A columns is achieved by a low pH wash which frequently leads to precipitation of HCP; if not during the elution itself, during the neutralization step following elution. Precipitation occurring inside the Protein A column can cause clogging and backpressure, impacting the resin lifetime. Due to the great expense of Protein A resins, decreasing resin lifetime will have large, negative

effects on process economics. Depth filters can effectively reduce HCP loads in harvested CHO cultures mitigating turbidity and precipitation issues during low pH processing conditions[21, 41]. Traditionally, cellulose fibers made up the filtration structure and diatomaceous earth was the filter aid of choice[18]. However, all-synthetic depth filters are becoming more common as they can be modified with more exploitative adsorption properties. Polyacrylic or polypropylene fibers interspersed with silica, activated carbon, or perlite filter aid provide filters increased process consistency, efficiency, and product quality[43] without leaching diatomaceous earth into the process stream[41].

2.1.2 Previous work

In this study, the performance of Millistak+ HC Pro X0SP 23cm^2 filters (Millipore Sigma, US) was evaluated. The pod filter module is made of a double layer of synthetic polyacrylic fibers with silica filter aid. It is marketed as providing enhanced HCP clearance for secondary clarification. Nguyen et al.[22], tested several mAbs after protein A chromatography on the X0SP filters and reported enhanced HCP removal by more than 10% in 3 out of the 6 cases, relative to X0HC filters which are comprised of cellulosic fibers with diatomaceous earth filter aid.

Preliminary testing of the Millistak+ HC Pro X0SP filters resulted in loss of mAb. In all these experiments, the filter was first flushed with DI water, then the harvested cell culture supernatant (HCCS) was loaded on the filter, followed by a buffer chase at different pH. The mAb recovery in the filtrate was calculated to be 76.5% with pure water chase, 50% with 20 mM sodium phosphate at pH 7 buffer chase, and 77.5% with 50 mM sodium acetate at pH 5 buffer chase respectively. From the preliminary work, water served as the best chase buffer for mAb

recovery. The objective of the following study is to further evaluate HCP and mAb recovery in filtrate fractions from varying ionic strength buffer chases.

2.2 Materials and methods

2.2.1 Cell growth

CHO cells obtained from Fujifilm Diosynth (FDB-01) were thawed from liquid nitrogen and transferred into 60 mL of CD OptiCHO media (Thermo Fisher, US) with 8µM glutamine and 75 µM methotrexate (MTX) at a seed cell density of 0.2x 10^6 cells/mL. This shake flask culture was considered thaw/passage 0 and grown at 140 rpm, 37°C and 5% CO_2 for 4 days. The cell growth and viability were measured by trypan blue staining and counting on TC20^{TM} cell counter (Bio-Rad, USA). When the cells reached >0.2x 10^7 cells/mL, they were passaged into 3 shake flasks, each with 60 mL of CD OptiCHO media, 8µM glutamine and 75 µM MTX at a starting cell density of 0.2x 10^6 cells/mL. This passage 1, was grown under the same physiological conditions till cell density reached >0.2x 10^7 cells/mL.

mAb production (passage 2) was done in 6 shake flasks each with 250 mL of CD OptiCHO media, 8µM glutamine at a seed cell density of 0.2x 10^6 cells/mL. Shake flask cultures were incubated at 140 rpm, 37°C and 5% CO_2 for 12 days. Cell boost 7A (10 mL) and 7B (1 mL) were fed to each flask on alternate days. The cell count and viability were monitored along with metabolites in the cell culture media using a NOVA Bioprofile 400 (Nova Biomedical, Waltham, USA) daily. When the glutamine and glucose concentrations dropped below 2.5 mM and 2 g/L respectively, the flasks were fed with 5 mM glutamine and 1 g of glucose solutions.

2.2.2 Harvest

On day 12 of the production flasks, the cell culture was aseptically transferred into harvest bottles and centrifuged at 500xg for 10 mins at 4°C. The supernatants were separated from the cell pellets and pooled. This was considered the harvested cell culture supernatant (HCCS) and used as the starting material for clarification by depth filtration.

2.2.3 Depth filtration

Spectrum Krosflow system was set up with Masterflex and Pharmed tubing (16mm i.d.). Millistak+ HC Pro X0SP 23cm^2 filter was connected to the system with pressure sensors on feed and filtrate lines. The filter was flushed with 120 mL DI water at 5.8 mL/min till the air was purged, then the flush flowrate was increased to 9.5 mL/min (250 LMH). Then. 250 mL of HCCS was filtered at 5.8 mL/min (150 LMH) followed by a chase with 120 mL of DI water as control. At the end of the experiment, the pump was allowed to run till the contents of the tubing and filter housing (hold-up volume) was also collected as a modified"blow-out" process. The filtrates of the flush, HCCS and chase were collected in 25 mL fractions. The experiment was repeated using a new filter with 0.5 M NaCl as chase buffer under the same operating parameters. The filtrates collected were stored at 4°C and analyzed for pH, conductivity, turbidity, total protein, DNA and mAb concentration.

2.2.4 Sample analysis

The total protein in samples were measured by 96-well microtiter method of Bradford assay (Pierce, Thermo Fisher) with BSA as standard. The double stranded DNA (dsDNA) concentration was measured by Quant-iT Picogreen dsDNA assay kit (Invitrogen, US) with

lambda phage DNA as standards. mAb and HCP concentration was measured by Poros-A XP column on Ultimate 3000 HPLC system. pH and conductivity of fractions were measured by Thermo Orion Star and Mettler Tolledo conductivity meters respectively.

2.3 Results and discussion

2.3.1 Preparation and characterization of feed material

Cell culture growth across multiple batches was monitored to ensure similar mAb production properties in absence of large-scale bioreactor. Multiple batches were scaled up and maintained at high viabilities until harvest. For each of the 6 production flaks, the cell count was monitored in quadruplets daily with TC 20^{TM} cell counter (BioRad, US). The viability of cells sizes between 7 to 22 μm were measured by trypan blue staining, where the alive cells rejected the stain and dead cells absorb trypan blue.

Over the span of 12 days, the CHO cells in all 6 flaks followed a similar growth pattern (***Figure 7***). They experienced lag phase for 4 days and then entered log phase, doubling approximately every 20-24 hours till day 8. Then, the cell density remained around 2 * 10^7 cells/mL and the cell viability started decreasing. It is expected that mAb production occurs during the stationary phase when the cells are under duress [44], so they were held till day 12, when the viability ranged from 75 – 85% and harvested by centrifugation.

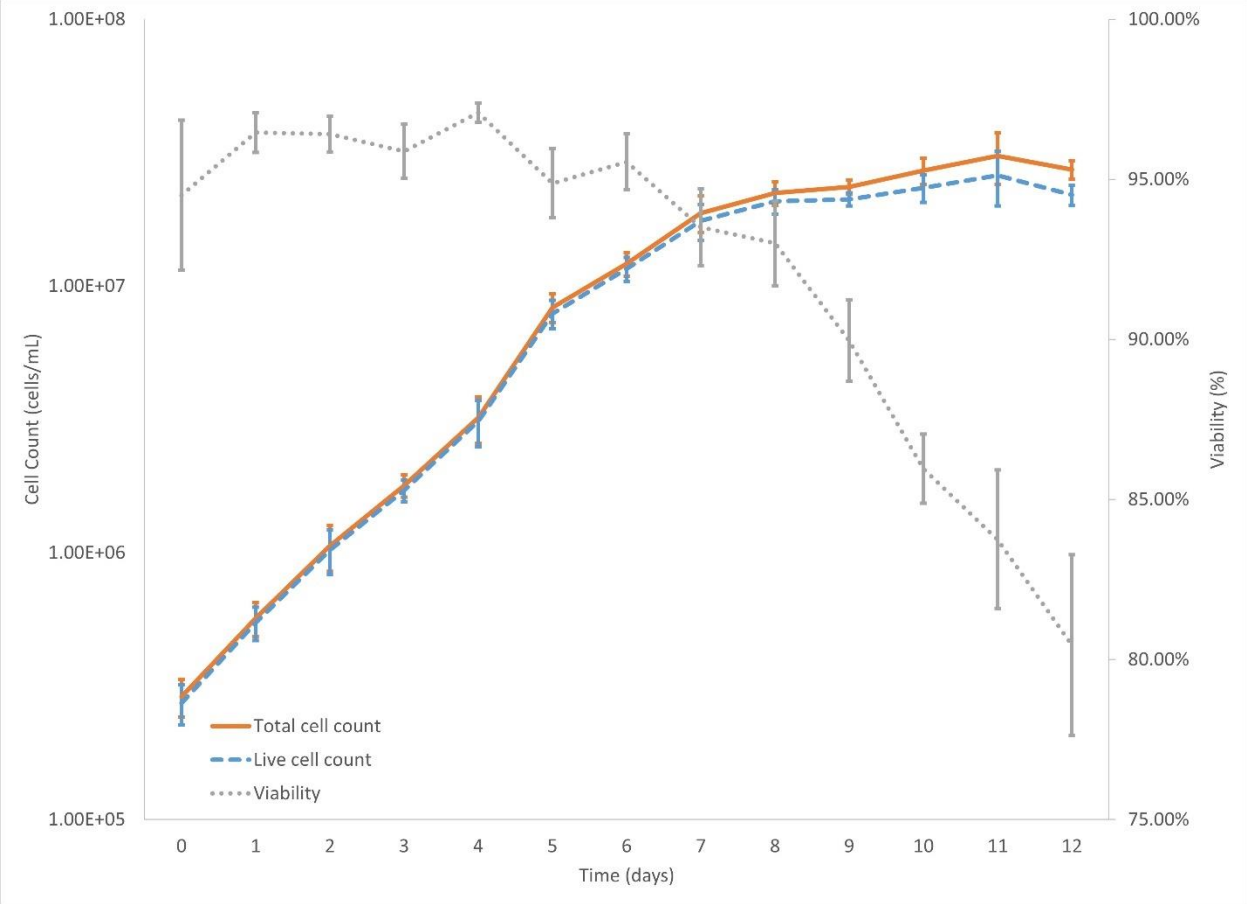

Figure 7 Growth curve showing total cell density, live cell density, and percent viability of CHO cells across production flasks

2.3.2 Monoclonal antibody expression

The production flasks did not contain methotrexate (MTX) in the serum-free growth media, encouraging the expression of mAb. The concentration of mAb in the cell culture supernatant was followed over time by HPLC analysis (***Figure 8***). mAb secretion began when the cells were in log phase (day 4), ranging from 0 – 0.5 mg/mL with the highest titers achieved in flask 5. In the late log and beginning of stationary phase (day 6-8), all the production flasks began to express mAb rapidly, which coincided with the rapid consumption of glucose and glutamine. These nutrients were fed when they dropped below the set threshold, to not increase the osmolarity and maintain low lactate and/or ammonia concentrations. This period from day 8 to

12, which corresponds to decrease in cell viability and metabolic stress on the CHO cells, has a rapid increase in mAb secretion every day [45].

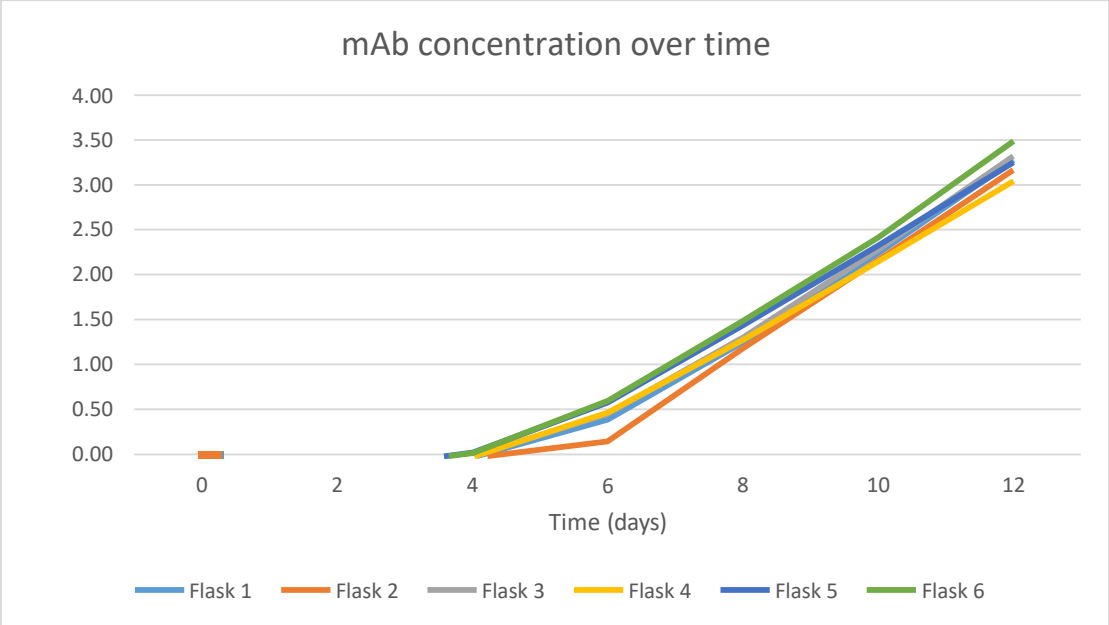

Figure 8 mAb concentration in cell culture supernatant of each production flask over the cultivation time

Despite the cells continuing to express mAb, they were harvested on day 12 to avoid further decrease in cell viability and release of associated HCP impurities into the cell culture supernatant [45]. The HCCS from each production flask was pooled, resulting in 1311.3g with 3.26 mg/mL mAb (***Table 1***).

Table 1 Harvested cell culture supernatant parameters individually and pooled

Flask #	Harvested weight (g)	pH	Conductivity (mS)	mAb conc. (g/L)
1	212.7	6.741	12.76	3.28
2	217.2	6.729	13.25	3.17
3	216.5	6.813	12.98	3.32
4	225	6.821	13.02	3.04
5	225	6.755	13.47	3.25
6	214.9	6.848	13.06	3.49
Pooled cell culture supernatant	1311.3	6.874	13.51	3.26

2.3.3 Depth filtration

Depth filtration was performed with the CHO HCCS. The filter was wet in the process of flushing with DI water, to condition the filter membrane. The start of the filtrate fraction collection was offset by ~35 mL to account for the buffer volume in the tubing or "hold-up volume". The flow parameters and pressure were monitored by the Spectrum Krosflow software. ***Figure 9*** displays the processing diagram of the depth filtration.

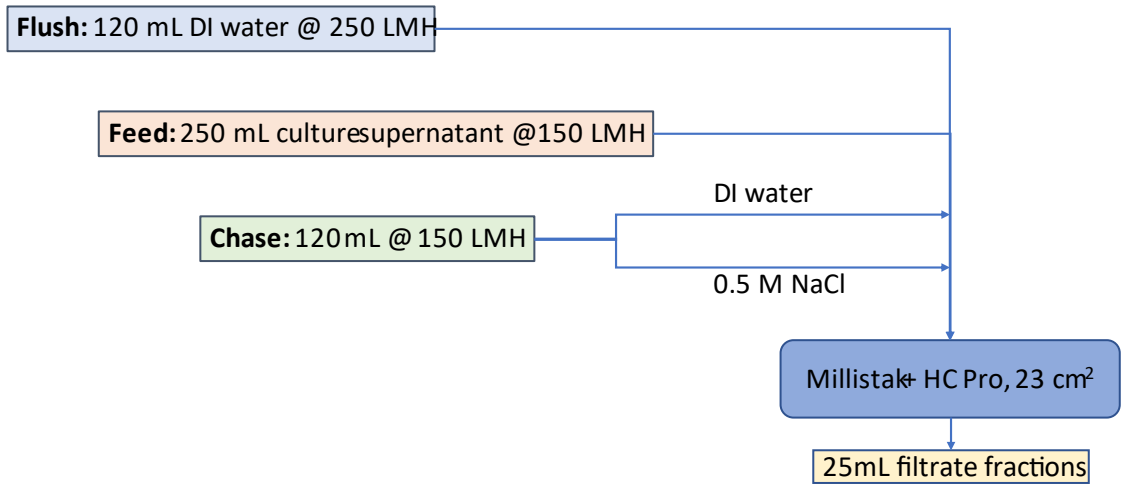

Figure 9 Flow diagram of the depth filtration experiments

2.3.3.1 Depth filtration with water chase

Figure 10a shows the flux rate over time for the control depth filtration with DI water as chase. The flux rate is 0 LMH until 13 mins, because the filter module is filling with DI water flush and purging out air. Once the air in the filter was eliminated, the flowrate was increased to 9.5 mL/min to speed up the flush process. This reflects as 250 LMH flux from 13 to 16 mins. During the depth filtration of the HCCS starting at 16 mins and the chase with DI water, the flux remains constant at 150 LMH. Since there was no drop in flux over the filtration of the feed, the filter is expected to be performing to its capacity without fouling. A further drop in flux is seen only towards the end of the DI water chase at 1h 18 mins when the contents left in the tubing and the filter were collected as a part of "blow out".

The pressure over time is shown in ***Figure 10b***. The transmembrane pressure (TMP) starts increasing to 2 psig after the filter was purged, when the flux of the flush was 250 LMH. During the HCCS filtration, a gradual increase in TMP was observed from 1.2 to 2.5 psig. The TMP only decreased marginally during the chase with DI water to 2.3 psig at 1h 12 mins. The chase DI water turned turbid when added to the feed tank. We hypothesis that the turbidity was

due to left over precipitated proteins from the HCCS [41], that could add to the pressure build up during the chase.

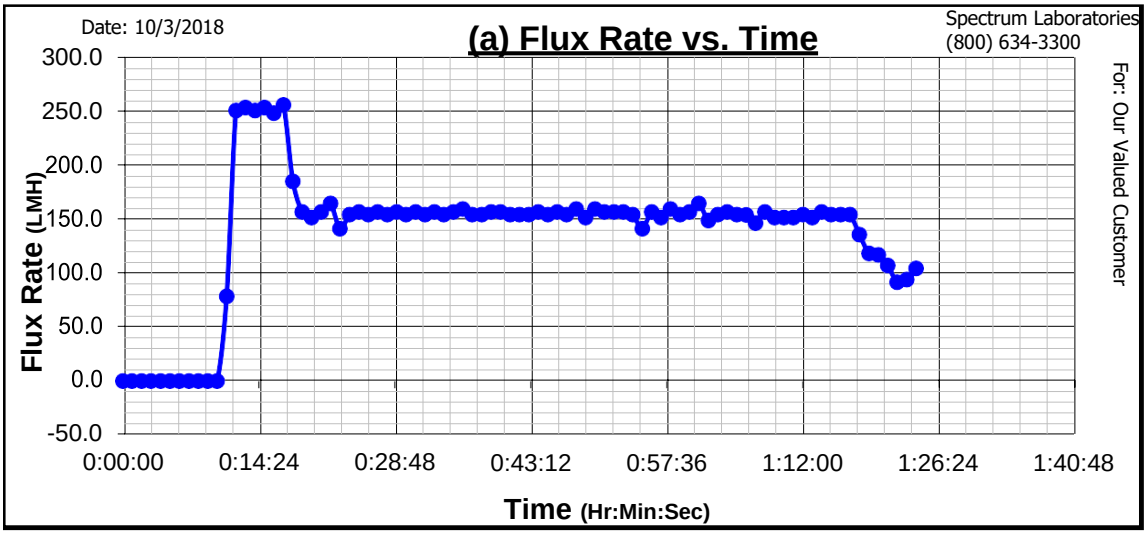

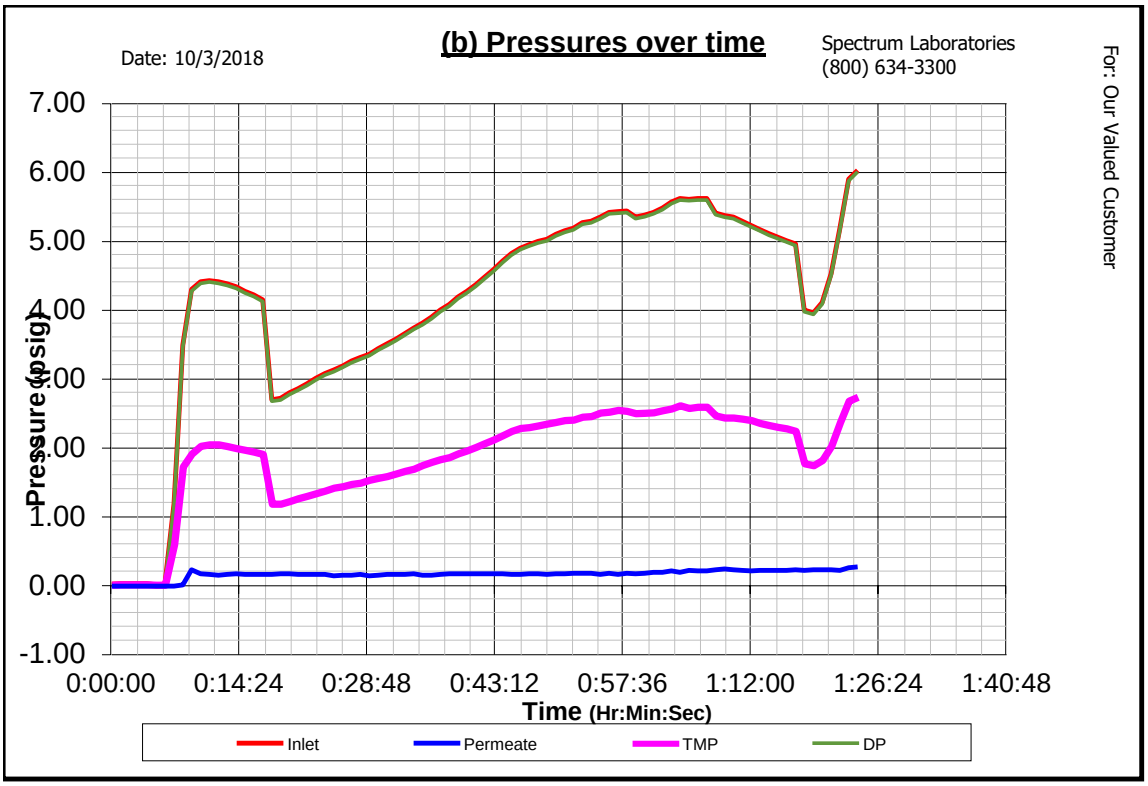

Figure 10 Real-time plots of flux (a) and pressure (b) over time during depth filtration experiment with DI water as chase

2.3.3.2 Depth filtration with 0.5 M NaCl chase

Similar to the depth filtration with water chase, the depth filtration with 0.5 M NaCl chase was performed and run data was collected (***Figure 11***). The flux rate of 300 LMH was observed after purging the filter, because the flow rate of the flush was increased to 13 mL/min. The filtration flux of the HCCS beginning at 15 mins and the chase with 0.5 M NaCl beginning at 57 mins were at 150 LMH. At the end of the chase, when the hold-up volume from the filters and tubing were collected, the flux started decreasing at 1h 18 mins.

The TMP over time (***Figure 11b***) followed a similar pattern in both experiments. The TMP reached 2.3 psig during the flush due to the higher flow rate. Similar to the previous experiment, gradual increase in TMP was observed during the filtration of HCCS from 1.2 to 2.5 psig. However, the 0.5 M NaCl chase was more effective in bringing down the TMP back to 1.8 psig at the end of the chase, compared to 2.28 psig at the end of DI water chase. This difference in the TMP during chase could be attributed to the lack of turbidity (or protein precipitation) when 0.5 M NaCl was added to the feed tank. Alternatively, 0.5 M NaCl chase could be more effective in releasing the components associating with the filter during the filtration of HCCS.

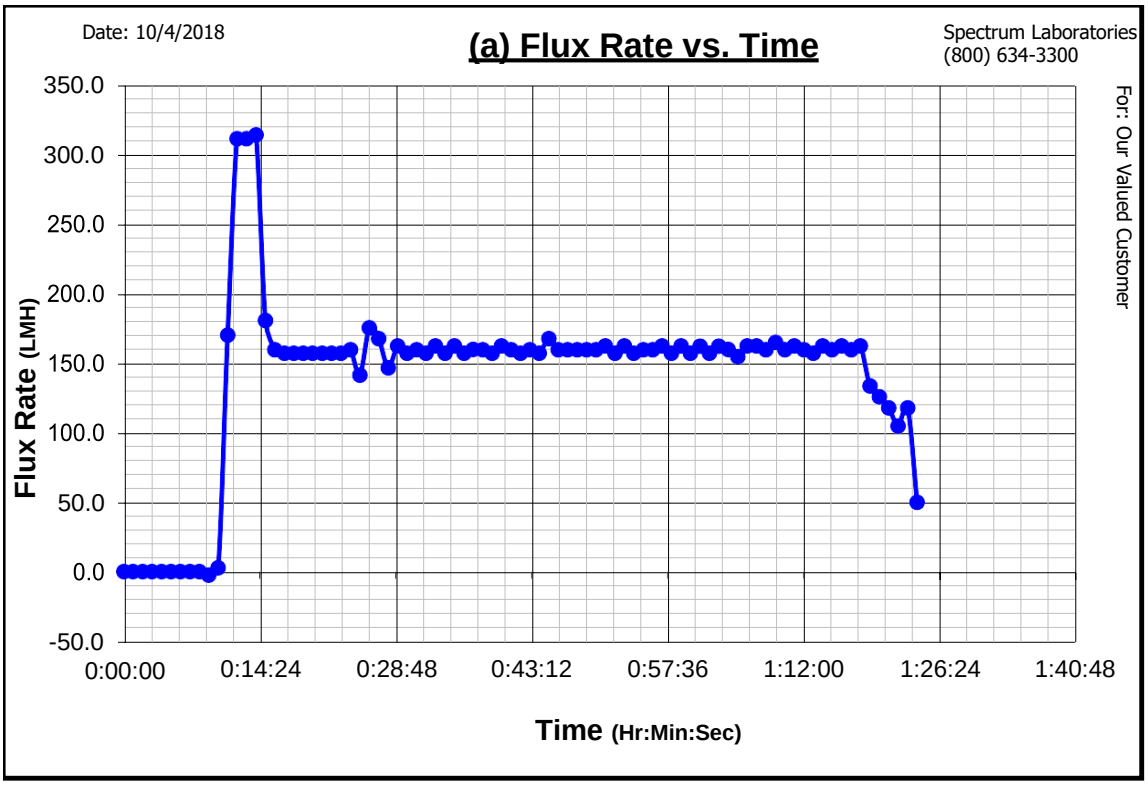

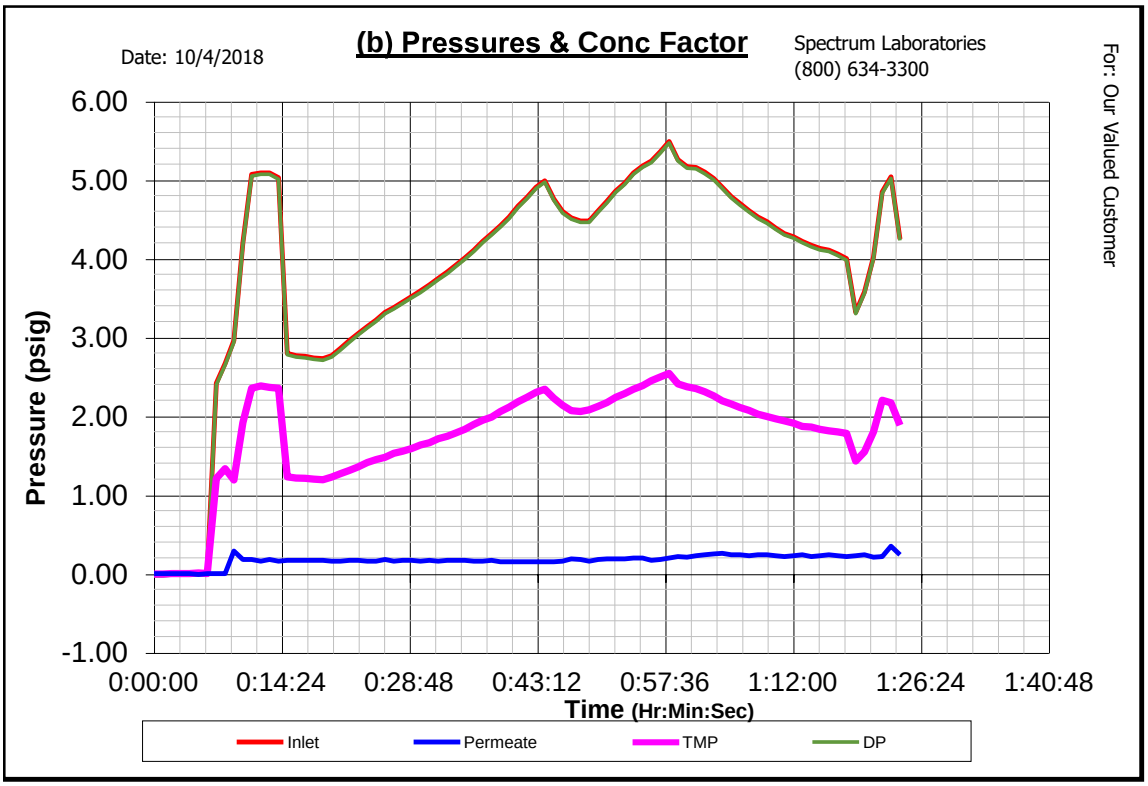

Figure 11 Real-time plots of flux (a) and pressure (b) over time during depth filtration experiment with 0.5 M NaCl as chase

2.3.3.3 Comparison of monoclonal antibody recovery

During both depth filtration experiments, the filtrates were collected in 25 mL fractions. The filtrate from the 120 mL DI water flush was collected, then 250 mL of the HCCS was filtered, the filtrate collected was called feed filtrate. Since there was no definite way of knowing when the feed filtrate emerged out of the filter, the hold-up volume in the tubing and filter housing was calculated approximately. The collection of feed filtrate was offset by the hold-up volume, and the 25 mL fractions were labelled numerically. The filtrates from the respective 120 mL chase buffer (DI water or 0.5 M NaCl) from each experiments were collected following the feed. The conductivity of all fractions was measured to obtain an insight into the mixing in the tubing and transition between buffers (***Figure 12a***). The filtrate fractions from both depth filtration experiments were analyzed for mAb concentration by HPLC and is shown in ***Figure 12b.***

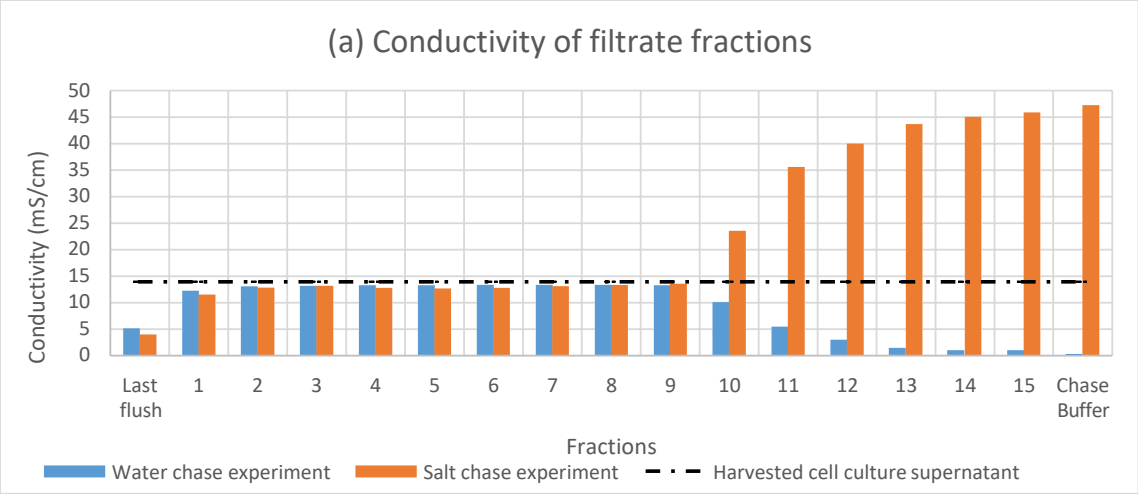

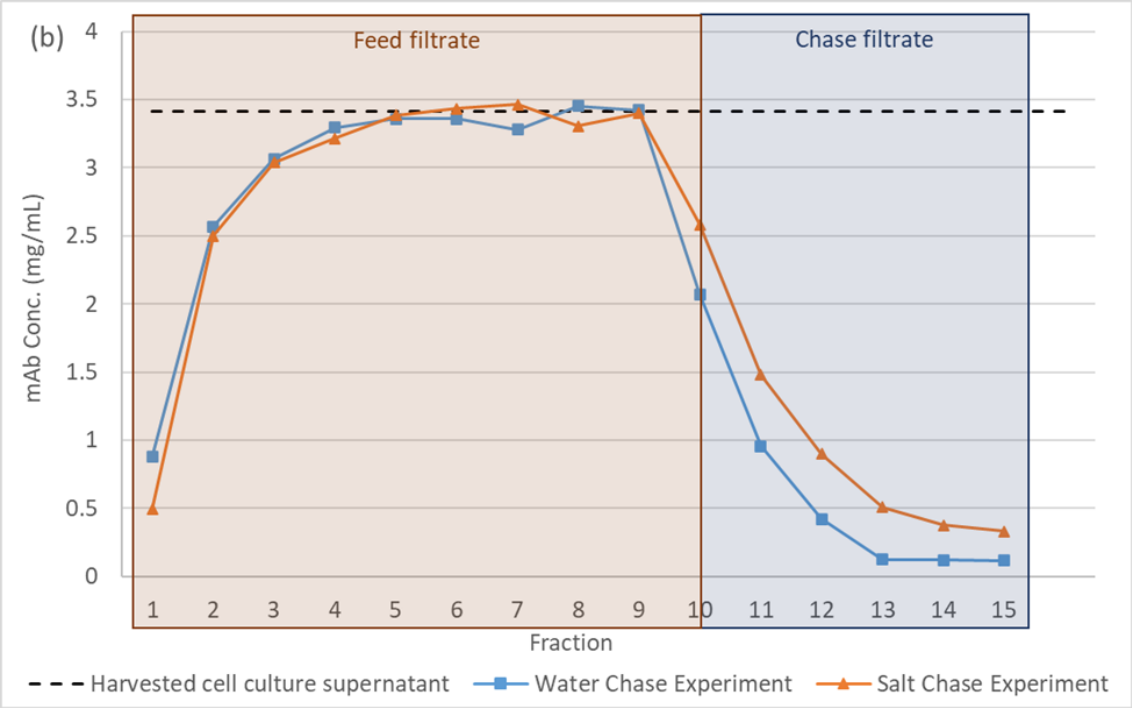

Figure 12 Conductivity (a) and mAb concentration (b) in filtrate fractions collected from depth filtration experiments

Since the fractions collected were by an approximate calculation of the hold-up volume in the filtration setup, the last flush fraction was included in the analysis to account for any feed filtrate that might have been collected in the earlier flush fractions. There was no mAb in the last flush fraction or it was below the detection limit of the HPLC, however the conductivity of the

fraction was >3 mS/cm in both experiments. This might be due to back mixing in the tubing during the transition of flush and feed, or the scale error while calculating the hold-up volume, resulting in excessive offset in the collection of filtrate fractions.

Then, the HCCS at 13.7 mS/cm conductivity and containing 3.39 mg/mL of mAb was filtered. Both experiments follow a similar pattern, filtrate fractions 1 to 3 have less than 3 mg/mL of mAb, this is attributed to the dilution of HCCS with the DI water from the flush, since the conductivity is less than 13 mS/cm. Feed filtrate fractions 4 to 9, contain ~3.3 mg/mL of mAb, similar to the starting concentration of HCCS, implying all mAb is recovered in these fractions. The conductivity of these fractions is in congruence with the HCCS.

Starting at fraction 10, the conductivity of the filtrate varies depending on the conductivity of the chase buffer used in each experiment. Fractions 10 to 12 of the feed filtrate have lesser than 3.39 mg/mL of mAb, again attributed to the dilution of the HCCS. However, a higher concentration of mAb is obtained in the experiment with 0.5 M NaCl chase. The difference in the mAb concentration between the two experiments, is shown in ***Figure 12b***.

The total mAb recovered in both experiments is shown in ***Table 2***. mAb recovery is 83.28% with the DI water chase compared to 86.79% with 0.5 M NaCl chase. Compared to the highest of 77.5% recovery in the preliminary experiments, the current recovery of 86.79% is significant improvement. The improvement in the recovery is attributed to the collection of the chase filtrate from the hold-up volume in the tubing and filter housing, in the form of a “blow out”.

Table 2 mAb recovered in depth filtration experiments

Sample	Water chase	0.5 M NaCl chase
mAb in feed (mg)	849	
mAb in filtrate (fractions 1-15) (mg)	707	737
% mAb recovery	83	87

2.3.3.4 Comparison of impurity removal

The host cell protein removal in both experiments were comparable, as shown in ***Figure 13*** and ***Table 3***. Only <10% of the proteins from the HCCS was removed during depth filtration.

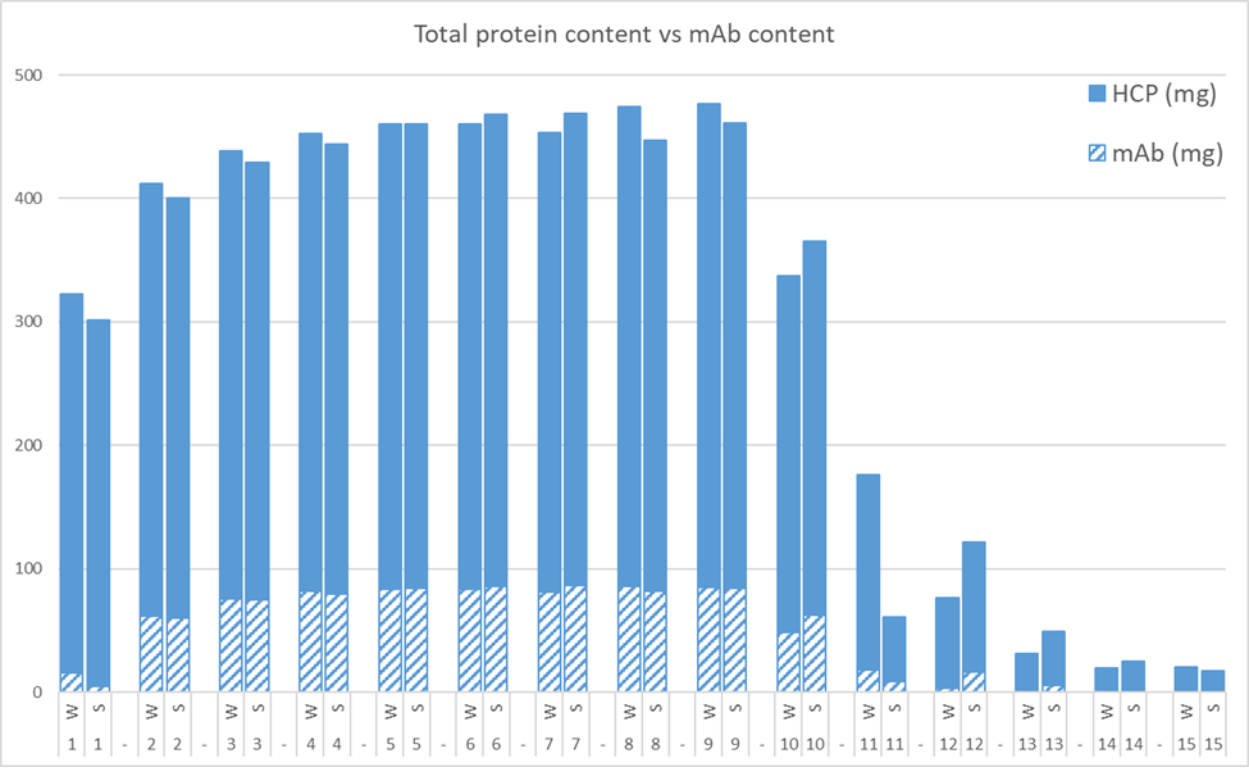

Figure 13 mAb and CHO cell protein (CHOP) distribution in each fraction collected from depth filtration

Table 3 Total protein and dsDNA content in the filtrate fractions from depth filtration

Sample	Water chase	0.5 M NaCl chase
Total protein in feed (mg)	4959	
Total protein in filtrate fractions (mg/mL)	4597	4518
% total protein recovery	93	91
Total dsDNA in feed (µg)	964	
dsDNA in filtrate fractions (µg)	43	79
% DNA recovery	4	9

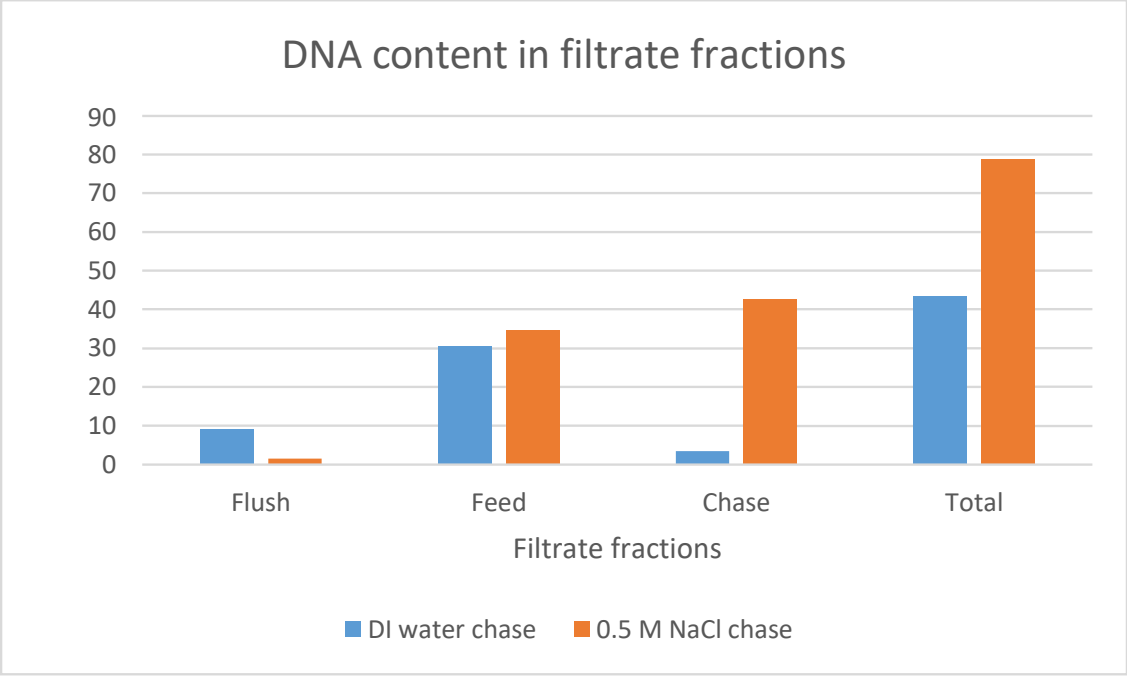

Figure 14 Double stranded DNA in the filtrate fractions of the depth filtration experiments

The dsDNA content in each of the filtrate fractions were quantified by Picogreen staining and shown in ***Figure 14*** and ***Table 3***. The depth filter is very effective in DNA removal, resulting in at least 10-fold reduction in dsDNA content. The flush and feed filtrate fractions

contain similar DNA concentrations. However, the 0.5 M NaCl chase buffer filtrates contain 42 µg of dsDNA compared to 3 µg of dsDNA in the DI water chase fractions (***Figure 14***). The higher conductivity of the chase buffer results in removal of feed DNA bound to the Millistak+ HC Pro X0SP filter. The elution of DNA could be the reason for the TMP recovering during 0.5 M NaCl chase.

Table 4 summarizes the outcomes of the depth filtration experiments using Millistak+ HC Pro X0SP filters and the effect of different chase buffers.

Table 4 Summary of mAb and impurities before and after the depth filtration experiments

Parameters	**HCCS**	**DI water chase experiment**	**0.5 M NaCl chase experiment**
mAb recovery (mg)	849	707	737
TMP after chase (psi)	-	2.3	1.8
HCP impurity (mg)	4959	4597	4518
dsDNA impurity (µg)	964	43	79

2.4 Conclusions

In this study, the 1.5 L of CHO cell culture was grown for 12 days with fed-batch nutrition supplementation and harvested before the cell viability dropped below 70%. Extending the growth period over 10 days resulted in additional mAb secretion, averaging 3.26 g/L.

The harvested cell culture supernatant was depth filtered for primary clarification using Millistak+ HC Pro X0SP 23cm^2. Two filtration experiments were performed, where 250 mL of HCCS was filtered, followed by 120 mL of DI water in one and 120 mL of 0.5 M NaCl in the second experiment, to enhance mAb recovery from the filter. Up to 86.79% of mAb could be

recovered, which was a 10% improvement from preliminary experiments. The additional recovery is attributed to the collection of "blow-out" chase filtrate from the hold-up volume of the filtration set-up. There was no significant difference in mAb recovered by the different chase buffers, implying that higher conductivity does not enhance release of mAb.

Finally, CHO cell protein (HCPs) impurity and DNA content of the filtrates were measured to test the impurity removal efficiency of depth filter. Up to 8% of the HCPs were removed by the depth filter but there was no significant difference between the two chase buffers.

Most importantly, the Millistak+ HC Pro X0SP filter facilitated dsDNA clearance of up to 96% at the current loading conditions. The chase buffer played a role in DNA removal, with 0.5 M NaCl chase eluting some dsDNA impurities bound to the filter. Based on the observation that both chase buffers result in similar mAb recovery and HCP removal (***Table 4***), but the DNA clearance could be the deciding factor on chase buffer selection. If DNA is detrimental to further processing steps, DI water is suggested as the chase buffer, to minimize DNA released from the filter. For all other cases, the 0.5 M NaCl chase buffer is recommended to maximize mAb recovery.

2.5 Recommendation for future work

Proper "blow-out" technique with forced air needs to be tested for enhanced mAb recovery. Investigation into the volumetric processing capacity of the filters and subsequent scale-up activities to replicate the observations of this study are highly recommended.

2.6 Acknowledgement

I would like to thank Alex Wood and Felipe Nicolau for their time and expertise in the growth of the cell culture; Dr. Ayswarya Ravi for assistance with experimentation and data collection; and Dr. Susan Woodard for helping with the analytical equipment. I am grateful to all the NCTM members for allowing the use of their facility and equipment for this study.

CHAPTER III

AGGREGATION TENDENCIES OF AFFINITY PURIFIED SPIKE PROTEIN VARIANTS

3.1 Introduction

A novel coronavirus, designated SARS-CoV-2, began circulating in December of 2019 resulting in mild to severe acute respiratory infections (coronavirus disease 2019 - COVID-19)[46]. This virus perpetuated very quickly throughout the human population, leading the World Health Organization to declare COVID-19 a global pandemic on March 11th, 2020[47]. Coronaviruses are a class of virions that have caused deadly outbreaks in the past such as SARS and MERS[48]. The SARS-CoV-2 virus shares roughly 80% sequence identity to the SARS-CoV virus that caused the SARS outbreaks of 2002 and 2003 and offered researchers a starting point in efforts to quell the spread of COVID-19[46].

The exterior of a coronavirus is covered with spike glycoproteins[48]. Each spike protein is a trimer comprised of three identical subunits containing a large ectodomain, a transmembrane anchor, and a small intracellular tail[48]. The receptor binding domain on the spike protein ectodomain attaches to the angiotensin-converting enzyme 2 (ACE2) receptor, undergoes a conformational change, and gains access to the cell[48-50]. For this reason, the spike protein has become the primary target for screening and development of neutralizing antibodies[50].

Screening for neutralizing antibodies that could become a prophylactic treatment requires large quantities of the antigen. To achieve this, the ectodomain of the spike protein was initially expressed transiently in HEK 293 cells for characterization and subsequently produced in stable HEK 293 and CHO cell lines. To achieve expression and detectable accumulation of the unstable SARS-CoV-2 protein, sequence modifications were made to the native spike protein ectodomain.

The modifications hold the spike protein in its prefusion conformation; the shape of the spike protein prior to fusion with the ACE2 receptor. Prefusion stabilization is beneficial for two main reasons: increased recombinant expression and heightened immunogenicity[51-53].

Modified spike protein constructs were created from residues 1-1208 of the native SARS-CoV-2 spike protein sequence (GenBank: MN908947)[54]. The base variant, S-2P, contains two consecutive proline substitutions at residues 986 and 987[50]. An improved variant, HexaPro, contains the same proline substitutions at 986 and 987 as well as four other proline substitutions at residues 817, 892, 899, and 942[50].Hsieh et al. (2020) compared the expression of four variants (Combo 14, 45,46, and 47) to that of S-2P and determined that the HexaPro variant (Combo 47) was the most stable with almost 10-fold higher expression level than S-2P.

Both variants (S-2P and HexaPro) also have "GSAS" substituted at the furin cleavage site, a C-terminal foldon trimerization motif, Human rhinovirus 3C (HRV3C) protease cleavage site, Twin-Strep-tag, and 8x His tag[50]. ***Figure 15*** details the SARS-CoV-2 spike protein wildtype sequence and differences of S-2P and HexaPro constructs.

Based on the number of amino acids in its sequence, a single spike subunit is estimated to be 142 kDa in size. Therefore, a full spike protein trimer should be roughly 426 kDa in size.

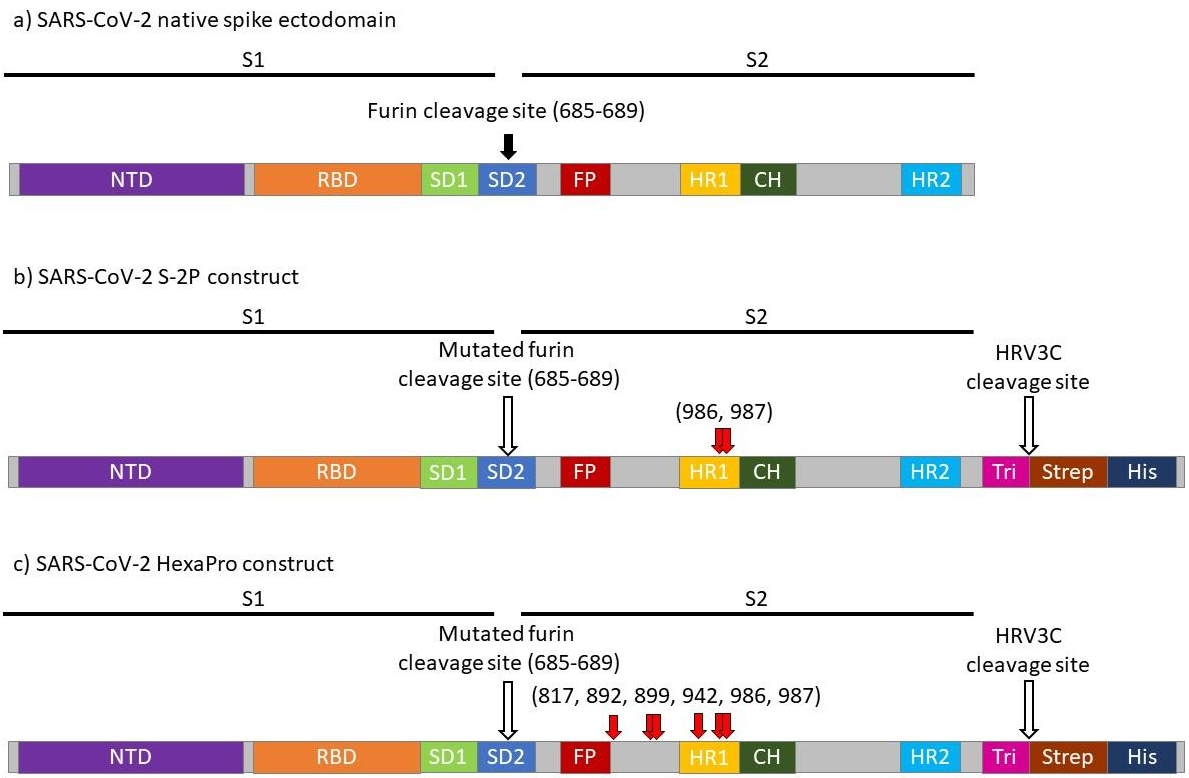

Figure 15 SARS-CoV-2 spike protein constructs N-Terminal domain (NTD), receptor binding domain (RBD), subdomain 1 (SD1) subdomain 2 (SD2), fusion protein (FP), heptad repeat 1 (HR1), central helix (CH), heptad repeat 2 (HR2), trimeric foldon region (Tri), Twin-Strep tag (Strep), 8x His tag (His); proline substitutions indicated with red arrows.

3.2 Materials and methods

3.2.1 Stable cell line growth

A 1 mL FreeStyle293F cell stock containing approximately 1×10^7 viable cells/mL expressing S-2P and/or HexaPro, obtained from collaborators at Army Research Lab – South, was thawed from liquid nitrogen in a 37°C bead bath for 2-3 minutes. The thawed culture stock and pre-warmed FreeStyle 293 Expression media (Thermo Fisher, US) were sprayed with 70% IPA and transferred into a biosafety cabinet along with a sterile, vented, non-baffled 125mL culture flask. The HEK293 stock was diluted into 29mL FreeStyle 293 Media for an approximate starting cell density of $2\text{-}3 \times 10^5$ viable cells/mL. The culture was capped and transferred out of

the biosafety cabinet into an incubator at 37°C with ≥80% humidity and 8% CO_2 on an orbital shaker at 120 rpm and was monitored every 24hrs until a cell density of 3×10^6 viable cells/ml was reached. A sterile, vented, non-baffled 1 L culture flask was prepared with 200mL of fresh, pre-warmed FreeStyle 293 Expression medium inside the biosafety cabinet. The initial seed culture was passaged into the fresh media for roughly 3×10^5 viable cells/mL and incubated at 37°C with ≥80% humidity and 8% CO_2 on an orbital shaker at 120 rpm and grown until they reached a cell density of 3×10^6 viable cells/ml with daily monitoring. This culture was passaged again into two larger sterile, vented, non-baffled 2.8 L culture flasks (Thomson, US) with fresh pre-warmed FreeStyle 293 Expression medium inside the biosafety cabinet to a total culture volume of 2.25 L at a seeding density of 3×10^5 viable cells/mL and incubated at 37°C with ≥80% humidity and 8% CO_2 on an orbital shaker at 120 rpm and grown until they reached a cell density of 3×10^6 viable cells/ml with daily monitoring. A final passage was performed with fresh pre-warmed FreeStyle293 Expression medium to bring total cell culture volume to 4 L and incubated at 37°C with ≥80% humidity and 8% CO_2 on an orbital shaker at 120 rpm and grown until they reached a cell density of 3×10^6 viable cells/ml with daily monitoring. Once the final culture volume was achieved, cultures were incubated at 37°C with ≥80% humidity and 8% CO_2 on an orbital shaker at 120 rpm and grown until viable cell readings dropped below 70% during daily monitoring.

3.2.2 Harvest

Viable cell count readings fell between 1-5e6 cells/mL at harvest. Once viable cell readings dropped below 75%, harvest was initiated. Cultures were transferred into centrifuge

bottles and spun at 15,900 × g at 4°C for 45 minutes. The supernatant was decanted into sterile bottles and the pelleted cells and debris were discarded.

3.2.3 Feed preparation

The harvested cell culture supernatant volume was estimated by its weight and an approximate density of 1.0 g/mL. The appropriate mass of sodium chloride (Sigma Aldrich, US) and imidazole (Sigma Aldrich, US) were weighed and added to the harvested supernatant to adjust the feed to 0.2 M NaCl and 10 mM imidazole respectively. A 0.45 μm mPES filter (Nalgene, US) was pre-wetted with 1x PBS prior to filtering the salt-adjusted feed material.

3.2.4 IMAC column packing and preparation

An AxiChrom 70/300 (Cytiva, US) column housing was packed with IMAC Sepharose 6 Fast Flow resin (Cytiva, US) to a bed height of 9.5 cm using the Intelligent Packing method wizard included in UNICORN Software (Cytiva, US) and AKTA Pilot Chromatography System (Cytiva, US). After confirming asymmetry and HETP values of the packed column were within acceptable ranges with a packing test in the downflow direction, the column was flushed with >2 CVs of DI water. Half a CV of a 0.2μm filtered 0.2 M nickel sulfate ($NiSO_4$) solution was applied to the column and then washed with at least 5 CVs of DI water to flush metal ions from interstitial spaces. A blank run was performed with 2 CVs of elution buffer: 50 mM sodium phosphate (Sigma Aldrich, US), 300 mM NaCl (VWR, US), 250 mM imidazole (Sigma Aldrich, US), pH 7.8; to remove weakly bound metal ions so that they do not co-elute with the product. The column was then equilibrated with at least 5 CVs of equilibration buffer: 50 mM sodium

phosphate, 300 mM NaCl, 20 mM imidazole, pH 7.8; until a stable baseline reading was reached at 220 nm. All column preparation steps were carried out at a linear flow rate of 150 cm/h.

3.2.5 IMAC purification

The filtered, salt-adjusted feed was loaded onto the equilibrated column via AKTA Avant 150 (Cytiva, US) and flowthough was fractionated and collected in 1L sterile bottles. Wash 1 was performed with 2 CVs of equilibration buffer: 50 mM sodium phosphate, 300 mM NaCl, 20 mM imidazole, pH 7.8; and Wash 2 was performed with 2 CVs of 78% equilibration buffer and 13% elution buffer: 50 mM sodium phosphate, 300 mM NaCl, 50 mM imidazole, pH 7.8 to desorb proteins with non-specific binding to the IMAC column. Flowthroughs for both washes were collected in 500mL sterile bottles. The elution step followed with 3 CVs of 13% equilibration buffer and 78% elution buffer: 50 mM sodium phosphate, 300 mM NaCl, 200 mM imidazole, pH 7.8; and was collected in 25mL fractions. Fractions corresponding to the elution peak were pooled. Wash 1, Wash 2, and the Elution step were all performed at 150 cm/h in the downflow direction while sample loading occurred at 90 cm/h in the downflow direction.

3.2.6 StrepTrap purification

A 1 mL Strep-Trap XT column (Cytiva, US) was attached to AKTA Avant 25 (Cytiva, US) and flushed with DI H2O before equilibrating with at least 5 CV of equilibration buffer: 100 mM Tris-HCl, 150 mM NaCl, 1 mM EDTA, pH 8. Harvested cell culture supernatant was loaded in the downflow direction and washed with 5 CV of equilibration buffer. Elution was achieved with 6 CV of elution buffer: 100 mM Tris-HCl, 150 mM NaCl, 1 mM EDTA, 50 mM biotin, pH 8. All steps were performed at 150 cm/h.

3.2.7 Buffer exchange by desalting column

A HiPrep 26/10 Desalting column (Cytiva, US) packed with Sephadex G-25 Fine resin and attached to ATKA Avant 25 (Cytiva, US) was utilized for desalting IMAC elution pool volumes of ≤ 30 mL. Pooled IMAC elution fractions were loaded into a cleaned and equilibrated 50 mL Superloop (Cytiva, US) to aid in sample loading. A 1x PBS running buffer was prepared from a 10x PBS stock solution (Alfa Aesar, US) and the column equilibrated for at least 5 CVs prior to sample loading. The void volume of the column, 15 mL, is also the maximum load volume and thus 15 mL was delivered to the column via the Superloop. After loading was complete, 2 CVs of running buffer followed to ensure all injected components passed through the column. If another load was required, 5 more CVs of running buffer was passed over the column before loading an additional 15 mL. Fractions were collected based on peak detection at A280.

3.2.8 Buffer exchange by membrane filtration

Tangential flow filtration was performed when IMAC elution pool volume was > 30 mL using a KrosFlo Research IIi TFF system (Repligen, US) and the coupled KF Comm software (Repligen, US). A 50 MWCO mPES hollow fiber membrane with 115 cm^2 filtration area (Repligen, US) was installed with sterile tubing and pressure sensors to monitor feed, permeate, and retentate pressure. Then it was prepared for use by flushing with at least 230 mL of DI water to rinse out the glycerin storage residue. A normalized water permeability (NWP) test was performed at the operating conditions to be used prior to sample loading to ensure the installed membrane was operating with appropriate permeability. If the NWP value was within the acceptable range, the pooled elution fractions were loaded into the feed reservoir and allowed to

recirculate through the hollow fiber membrane and back into the retentate vessel at low flow rate with no back pressure applied and permeate line closed. Product concentration began when the permeate stream was opened, flow rate increased to 75 mL/min, and transmembrane pressure (TMP) set to 1.5 psig. The processing volume was concentrated roughly 6-fold before a constant-volume diafiltration began. Once the diafiltration line was added to the retentate vessel, a vacuum was created and responsible for pulling in the equivalent amount of diafiltration buffer as liquid leaving the permeate stream. Five diafiltration volumes of 1x PBS, pH 7.4 (Alfa Aesar, US), was introduced to drop imidazole concentration below 2 mM. To end the TFF run, the flow rate was stopped, back pressure turned off, permeate stream closed, and pump direction reversed to recover all liquid in the retentate vessel.

Smaller volumes of IMAC elution pool were concentrated and diafiltered using Macrosep Advance centrifugal devices with mPES 30MWCO membrane (Pall, US). IMAC elution pool sample was loaded into the top reservoir of the filtration device, placed in 45° fixed angle rotor, and centrifuged at 5000xg at 4°C in 5-minute intervals until the samples were concentrated to roughly 1 mg/mL protein. Then, five diafiltration volumes of 1x PBS buffer (Alfa Aesar, US) was introduced to the sample reservoir and again spun at 5000xg at 4°C in 5-minute intervals to reduce imidazole concentrations.

3.2.9 Protease cleavage

An HRV3C protease was obtained from our collaborators at the Army Research Lab South. This protease is His-tagged. The HRV3C protease was added to spike protein samples in a mass ratio of 1:50. Samples were incubated overnight at 4°C. To recover just the cleaved spike protein, the entire sample was again loaded on an IMAC column. The cleaved His-tags as well as

the His-tagged protease bound to the IMAC column and the tail-free spike variant was collected in the flow through fraction of sample loading.

3.2.10 Protein concentration by ultraviolet absorbance

After imidazole removal, the concentration of protein was estimated by absorbance at 280 nm. The spectrophotometer (Beckman Coulter DU730 UV/Vis Spectrophotometer, US) was blanked with 1x PBS before reading unknown samples. All measurements were performed in a quartz cuvette. Blank-adjusted absorbance values were converted to protein concentration by the following equation:

$$Conc\left[{}^{mg}/_{mL}\right] = (A_{280}) \times (molecular\ weight\ [Da])/(\epsilon_{280})$$

where the extinction coefficient, ϵ_{280}, is amino acid sequence dependent based on the following equation:

$$\epsilon_{280} = 5500W + 1490Y + 125C$$

where W is the number of tryptophan residues, Y is the number of tyrosine residues, and C is the number of cystine residues. The extinction coefficient used for all spike protein variants was calculated to be 146845 M^{-1} cm^{-1}.

3.2.11 Protein concentration by ELISA

For concentration determination of samples with imidazole, an enzyme-linked immunosorbent assay (ELISA) was developed. A NUNC Maxisorp Flat Bottom Immuno 96-well plate (ThermoFisher, US) was coated with 100 µL/well of capture antibody, SB40150-D0003 (Sino Biological, US), diluted 1:5000 in 0.22µm filtered 1x PBS (Alfa Aesar, US). The plate was covered with an acetate plate sealer (MP Biomedicals, US) prior to overnight storage at 4°C. The

following day, the plate was blocked with 100 µL/well of 5% powder non-fat milk in 1x PBS with 0.05% Tween-20 (1x PBS-T) applied on top of the coating solution already in the wells. The plate was incubated at room temperature for 2 hrs prior to washing. A Biotek ELx50 Microplate washer (Agilent, US) was primed with 1x PBS-T to wash the wells 3 times with 250 µL of PBS-T for each wash. Standards and unknown samples were diluted into 1x PBS-T with 1% BSA before applying 100 µL to the washed plate and incubating at room temperature for 2 hrs. The plate was washed again 3 times/well with 250 µL of 1x PBS-T. The detection antibody, SB40150-D001-H (Sino biological, US), was diluted 1:5000 in 1x PBS with 1% BSA before applying 100 µL per well and incubating at room temperature for 1 hour protected from light. The plate was washed 4 times per well with 300 µL of 1x PBS-T. TMB substrate solution (ThermoFisher, US) was applied at 100 µL per well and allowed to develop ntil color was visible in the lowest standard of the standard curve. The substrate reaction was stopped with 100 µL of 0.2 M sulfuric acid applied per well. The plate was read at 450 nm with a 650 nm reference wavelength on a BioTek Synergy H1 plate reader (Agilent, US) with BioTek Gen 5.2 software for data analysis.

3.2.12 SDS-PAGE

Spike protein samples were prepared with 4x Laemmli Sample Buffer (Bio-Rad, US) in 3:1 ratio prior to heating on a heat block at 95°C for 7 minutes. Reduced spike protein samples were prepared nearly identically with the addition of 10% 2-mercaptoethanol (BME) (Thermo Fisher, US) to the 4x Laemmli Sample Buffer prior to incubation with the sample. One liter of 1x Tris/ Glycine/SDS running buffer was prepared from 10x Tris/Glycine/SDS stock (Bio-Rad, US) and placed in 4°C to chill. A 4-15% Mini-PROTEAN TGX precast gel (Bio-Rad, US) was

unwrapped, the comb and the sticker removed, and setup in the gel holder of a Mini-PROTEAN Tetra Vertical Electrophoresis Cell (Bio-Rad, US). The integrity of the gel holder seal was tested with running buffer and if no leaks were present, running buffer was added to the outer chamber of the gel box to the designated line. Up to 28 μL of sample and 10 μL of standard were loaded into wells before carefully fitting the lid onto the gel box. The electrophoresis cell was plugged into a PowerPac Universal Power Supply (Bio-Rad, US) and set to constant 150V for 50 minutes. Once the run was completed, the gel holder was removed and dismantled, the gel cassette was broken apart, and the gel was transferred into a container with DI H_2O and shaken gently. From here, the gel was either stained or blotted using one of the following protocols.

3.2.13 Blue native PAGE

Non-reduced spike protein samples were prepared with 4x BN PAGE Sample Buffer (Thermo Fisher, US) in a 3:1 ratio with the addition of 20x BN PAGE Cathode Additive (Thermo Fisher, US) and incubated. Reduced spike protein samples were prepared nearly identically with the addition of 10% 2-mercaptoethanol (BME) (Thermo Fisher, US) to the 4x BN PAGE Sample Buffer prior to incubation with the sample. A NativePAGE 4-16% Bis-Tris Protein Gel (Thermo Fisher, US) was assembled into a XCell SureLock Mini-Cell (Invitrogen, US) electrophoresis system and loaded with prepared samples. A constant 150V was applied for 105-120 minutes; runs were stopped when the dye front reached the last quarter of the gel. Once the run was completed, the gel holder was removed and dismantled, the gel cassette was broken apart, and the gel was transferred into a container with DI H_2O and shaken gently before staining.

3.2.14 Gel staining with coomassie

After thoroughly rinsing the gel in DI H_2O to remove any remaining SDS, enough Bio-Safe Coomassie stain (Bio-Rad, US) was applied to just barely cover the gel before placing on gentle shaking platform for 1 hour. Stain was removed and copious DI H_2O added to destain the background. Water was changed at least every 30 minutes while shaking. Gels were imaged using the ChemiDoc System (Bio-Rad, US) once water changes ran clear and there was significant contrast between background and protein bands.

3.2.15 HPLC SEC

A Superose 6 Increase 10/300 column (Cytiva, US) was attached to an AKTAmicro (Cytiva, US) chromatography system. Five protein standards; thyroglobulin, ferritin, aldolase, conalbumin, and ovalbumin; were prepared to create a calibration curve. A running buffer of 10 mM phosphate, 140 mM NaCl, pH 7.13 was prepared and used to equilibrate the column after copious amounts of DI H_2O flushed out the storage buffer. Samples of 100 µL were injected after a stable baseline was observed. The flowrate was maintained at 0.5 mL/min. The known molecular weights of the standards and their corresponding retention volume was utilized in the below equation to generate a calibration curve [55].

$A = A_o e^{-kr}$ where $r = V_e/V_o, V_e = retention\ volume, V_o = void\ volume, A = MW(kDa)$

3.3 Results and discussion

3.3.1 Downstream processing of spike protein variants

Batches of recombinantly produced COVID-19 spike protein variants were purified following the block diagram depicted in ***Figure 16***.

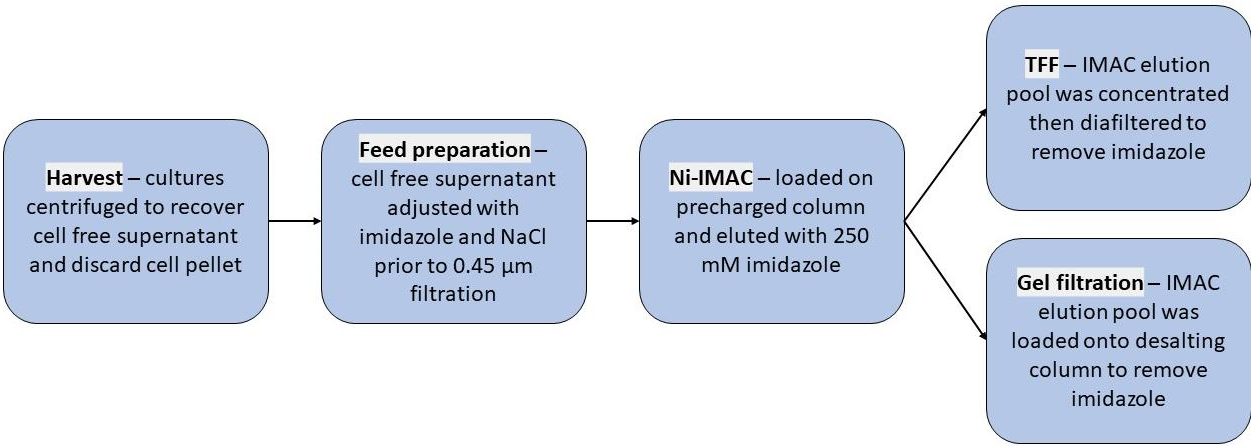

Figure 16 Purification block diagram for recombinant SARS-CoV-2 spike protein variants

Cell cultures were harvested at relatively low RPM that was sufficient to remove mammalian cells but avoid unintentional cell lysis. The cell-free supernatant was conditioned with 10 mM imidazole and 200 mM NaCl to minimize non-specific binding on the affinity column. The filtration after feed adjustment prevents cells, debris, or large colloidal material from entering the column and protects its lifespan. Depending on the harvested volume, either an AxiChrom 50/300 or AxiChrom 70/300 was selected to optimize the total run time while maintaining at least 5 minutes of residence time during loading. Clarified supernatant was loaded onto a nickel-charged IMAC column where it was washed once with equilibration buffer containing 20 mM imidazole, then washed with 50 mM imidazole, and eluted with 250mM imidazole. ***Figure 17*** represents a typical IMAC purification chromatogram for an S-2P batch.

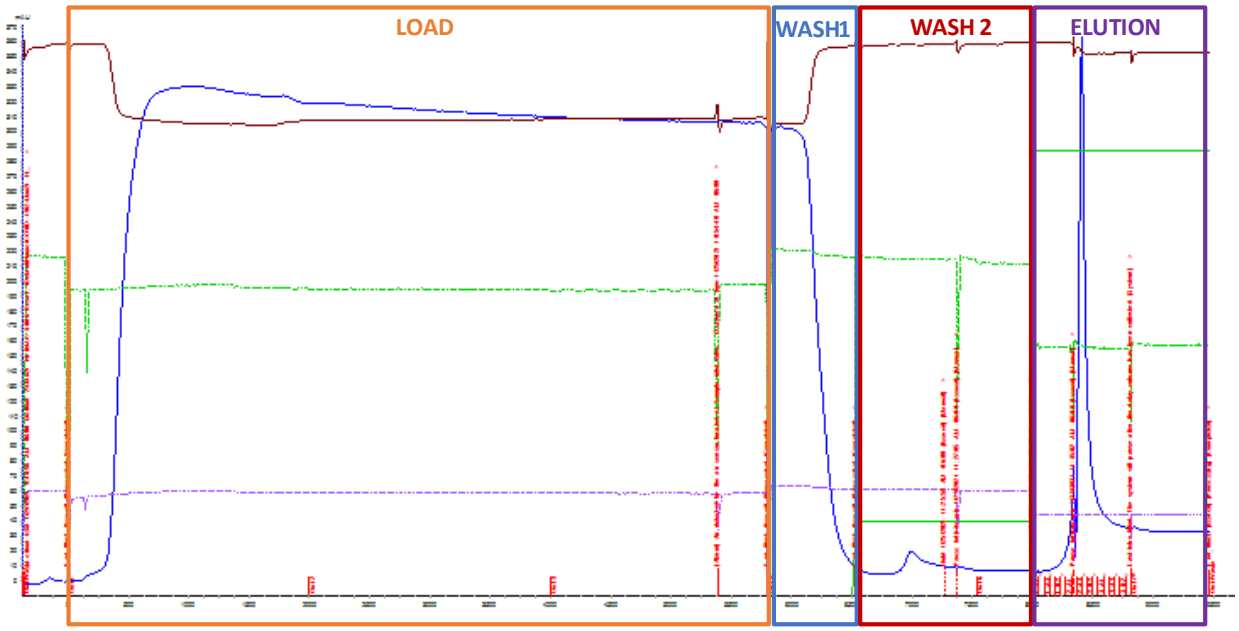

Figure 17 Chromatogram of IMAC purification (blue line – A280; brown line – conductivity; solid green line – concentration of buffer B; dotted green line – precolumn pressure; dotted lavender line – delta column pressure)

Imidazole is incompatible with many assays for quantification (UV-Vis spectroscopy, ELISA reagents, etc.) therefore its removal was necessary. To remove imidazole from the IMAC elution pool, three different methods were applied. Buffer exchange was performed using centrifugal concentration tubes ("spin tubes") (Pall, US) when the pooled IMAC elution fraction was 6 mL or less and SEC using a gel filtration column (Cytiva, US) when the pooled IMAC elution fraction was between 6 – 30 mL. For larger volumes, TFF was performed to both 1) concentrate IMAC elution fractions and 2) exchange buffer conditions. In several instances, we observed an increase in visible turbidity at the onset of diafiltration on TFF. This turbidity was never observed in fractions from the gel filtration column or with centrifugal concentration tubes. This observation seems to indicate that in absence of a pumping action, proteins were less prone to aggregation. In all cases, protein samples that were exposed to shear during recirculation in the TFF unit had visible turbidity (***Table 5***). The protein concentration does not seem to be the

reason for the observed turbidity as spin tube concentration and diafiltration did not result in turbidity at 11 or 33 mg/L respectively, whereas TFF produced turbid samples at both concentration levels. The results of purification of five S-2P and two HexaPro batches are summarized in ***Table 5***.

Table 5 Characteristics of S-2P and HexaPro spike variants during processing

Construct and Harvest date	**Final culture volume (mL)**	**Theoretical Production level (mg/L)**	**Buffer Exchange method**	**Post Buffer exchange Turbidity**
S-2P (Aug 14)	1,951	13	TFF	Yes
S-2P (Oct 11)	1,560	11	Desalt column	No
S-2P (Oct 15)	2,051	11	TFF	Yes
S-2P (Nov 6)	483	11	Spin tubes	No
S-2P (Jan 24)	5600	12	TFF	Yes
HexaPro (Sept 16)	746	33	Desalt column, spin tubes	No
HexaPro (Sept 20)	1,980	37	TFF	Yes

Production level (mg/L) is an estimate of the spike protein titer in the harvested culture media based on the purified and desalted amount of spike variant assuming 100% recovery. The S-2P spike protein variant theoretical titers fell between 11-13 mg/L while the HexaPro variant theoretical titers were about 33 and 37 mg/L. Greater accumulation of HexaPro than S-2P was anticipated and correlated well to the SDS-PAGE data in ***Figure 18a***. Significantly thicker bands of HexaPro compared to S-2P are in indication of greater protein accumulation of HexaPro

variants. The protein yield of the IMAC chromatography step was about 70% for both spike variants.

Figure 18a, shows an SDS-PAGE comparison of protein expression levels for the variants assessed by Hsieh et al., 2020 [50]. ***Figure 18b,*** compares UV 280 detector response (mAU) of purified variants that were analyzed by SEC. There is notable difference of expression levels between S-2P (black line) and HexaPro (green line) confirming the SDS-PAGE data in ***Figure 18a***[50].

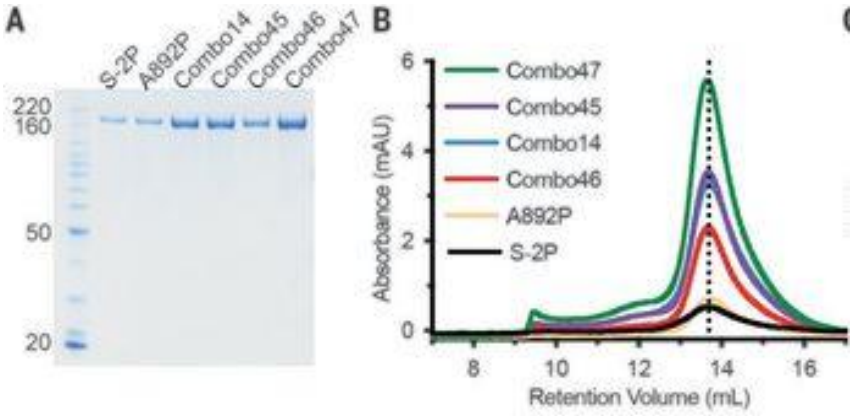

Figure 18 SDS-PAGE and HPLC SEC analysis of SARS-CoV-2 spike protein variants(a) SDS-PAGE of spike protein variants and molecular weight standards (b) size exclusion chromatography traces for many combo variants; the vertical dotted line indicates the peak retention volume for S-2P – Reproduced with permission from [50]

3.3.2 Analysis of purified and dialyzed spike protein variants by PAGE

Purification efficiency of S-2P variant was assessed at first by SDS-PAGE. ***Figure 19*** shows the progression of purity from the cell-free HEK293 culture in lanes 1 and 5, to highly purified IMAC pools (lanes 2 and 6). The samples in lanes 3 and 7 correspond to reduced and non-reduced IMAC pools after the desalting steps. The nonreduced samples in lanes 1, 2, and 3 seem to have a slightly lower MW than those that were reduced. Because the reducing step did not generate additional protein bands, and unexpectedly resulted in a slight MW increase, it was

concluded that the MW discrepancy was an artifact. The estimated protein monomeric MW of ~150 kDa from the SDS-PAGE corresponds reasonably well to expected 160 kda size.

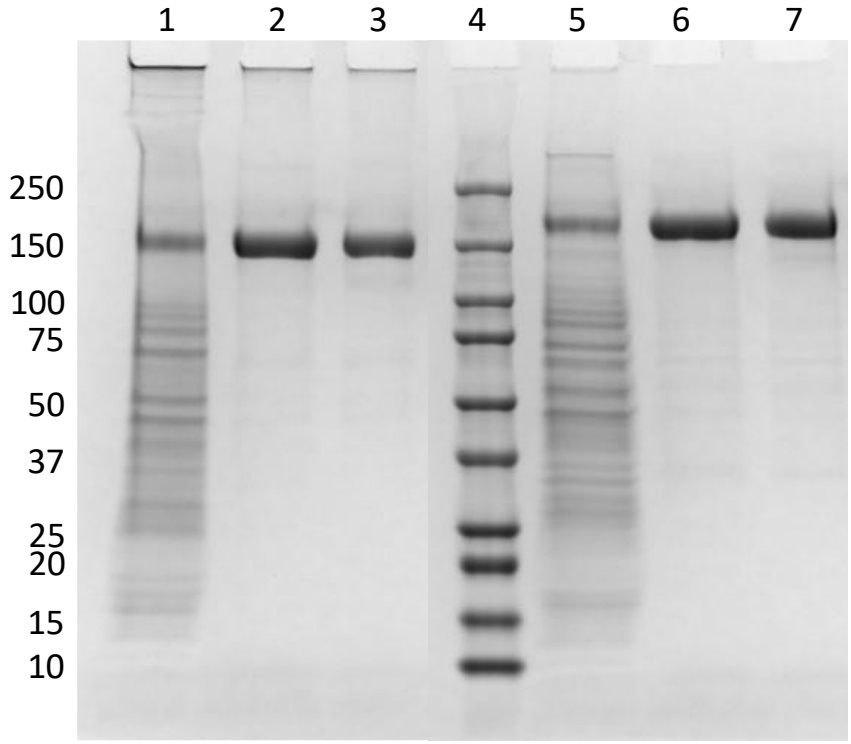

Figure 19 Coomassie Blue Stained SDS-PAGE of S-2P samples during processing steps (Lane 1: culture harvest – nonreduced; Lane 2: IMAC elution pool – nonreduced; Lane 3: Desalt pool – nonreduced; Lane 4: Molecular weight marker; Lane 5: culture harvest – reduced; Lane 6: IMAC elution pool – reduced; Lane 7: Desalt pool – reduced)

A different picture emerged when the same samples were analyzed by a native PAGE (***Figure 20***). Instead of anticipated 480 kDa bands corresponding to the trimeric S-2P size, the same samples analyzed by a Blue-Native PAGE, appeared to be mostly aggregated trimers roughly 1000 kDa in size. Only boiling the reduced IMAC EP sample (lane 8 **-** ***Figure 20***) managed to produce trimeric S-2P.

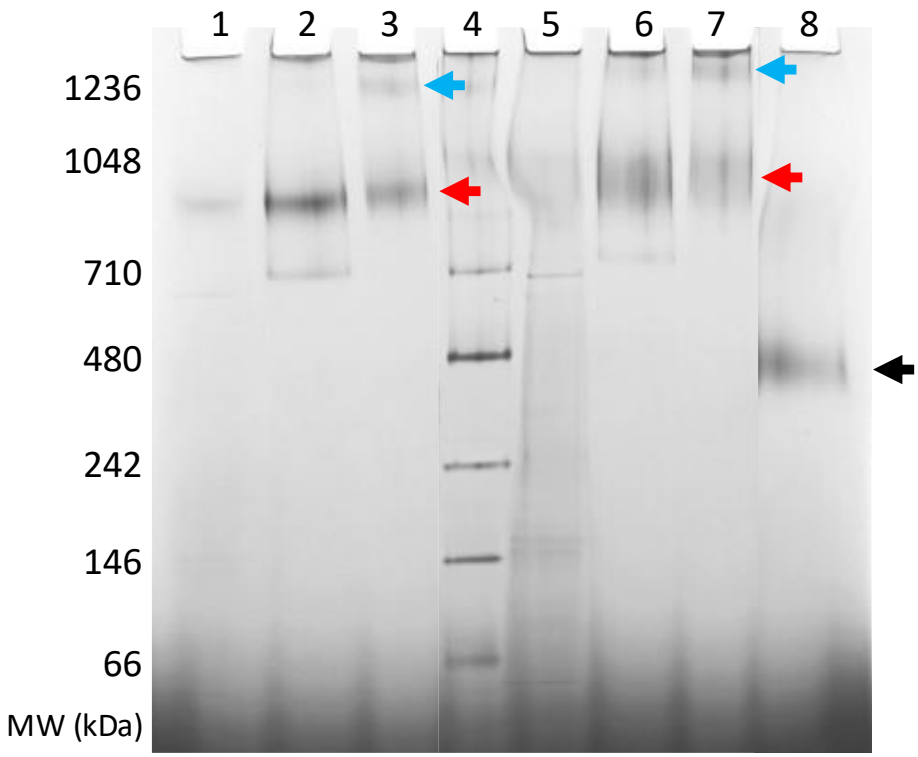

Figure 20 Coomassie Blue stained BN-PAGE of S-2P samples during processing steps: black arrowhead – single spike protein trimer; red arrowheads – dimer of spike protein trimer; blue arrowheads – trimer of spike protein trimers (Lane 1: culture harvest – nonreduced; Lane 2: IMAC elution pool – nonreduced; Lane 3: Desalt pool – nonreduced; Lane 4: Molecular weight marker; Lane 5: culture harvest – reduced; Lane 6: IMAC elution pool – reduced; Lane 7: Desalt pool – reduced; Lane 8: IMAC elution pool BOILED - reduced)

Because turbidity was observed during diafiltration on a tangential flow filtration unit, the retentate from TFF was centrifuged to pellet out insoluble 'cloudy' material. The left-over pellet was resuspended in diafiltration buffer and ran on SDS-PAGE to assess composition and purity of the turbid pelleted material. The resulting SDS-PAGE is shown in ***Figure 21***. Lanes 3 and 8 on ***Figure 21*** are the resuspended pellet sample non-reduced and reduced, respectively. While degradation products are also present in the pelleted protein material, the majority of the pelleted has the proper molecular weight for the S-2P monomer (~150 kDa). This result indicates that the source of the observed turbidity was in fact S-2P protein.

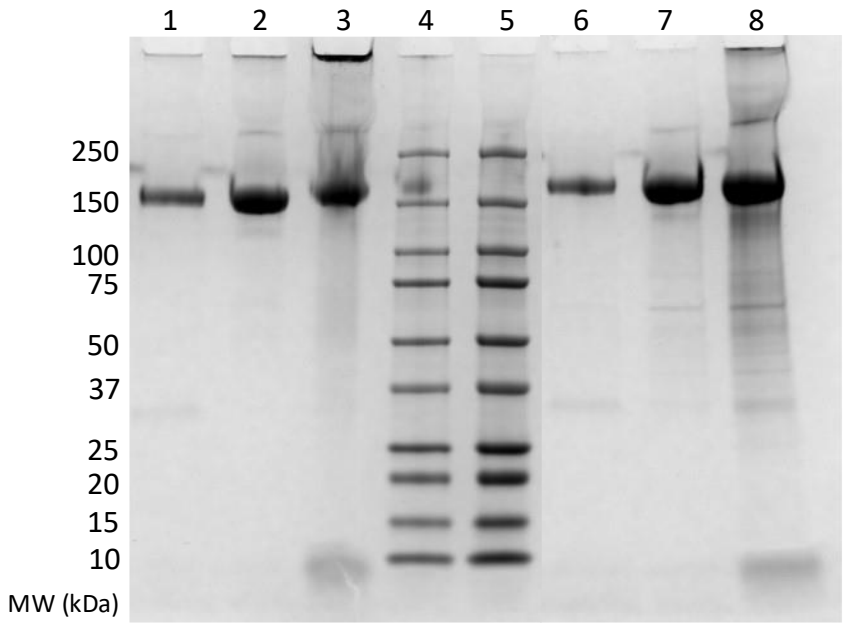

Figure 21 Coomassie Blue Stained SDS-PAGE of S-2P samples during IMAC and TFF processing steps (Lane 1: IMAC elution pool – non-reduced; Lane 2: TFF retentate centrifuged supernatant – non-reduced; Lane 3: TFF retentate centrifuged pellet resuspended – non-reduced; Lane 4: Molecular Weight marker (5 µl); Lane 5: Molecular Weight marker (10 µl); Lane 6: IMAC elution pool – reduced; Lane 7: TFF retentate centrifuged supernatant – reduced; Lane 8: TFF retentate centrifuged pellet resuspended – reduced)

3.3.4 Analysis of purified and dialyzed spike protein variants by SEC

To further assess the quality of purified spike protein variants (purity, aggregation, and degradation), size exclusion chromatography was employed. Protein standards across the MW range of S-2P monomers, dimers, trimers, and potential aggregates were injected on the sizing column attached to UV 280 and 220 nm wavelength detectors. The chromatograms in ***Figure 22*** were analyzed; coupling retention volumes with void volume information for each standard of known size, a MW calibration curve was generated (***Figure 23)*** for the Superose 6 Increase 10/300 column.

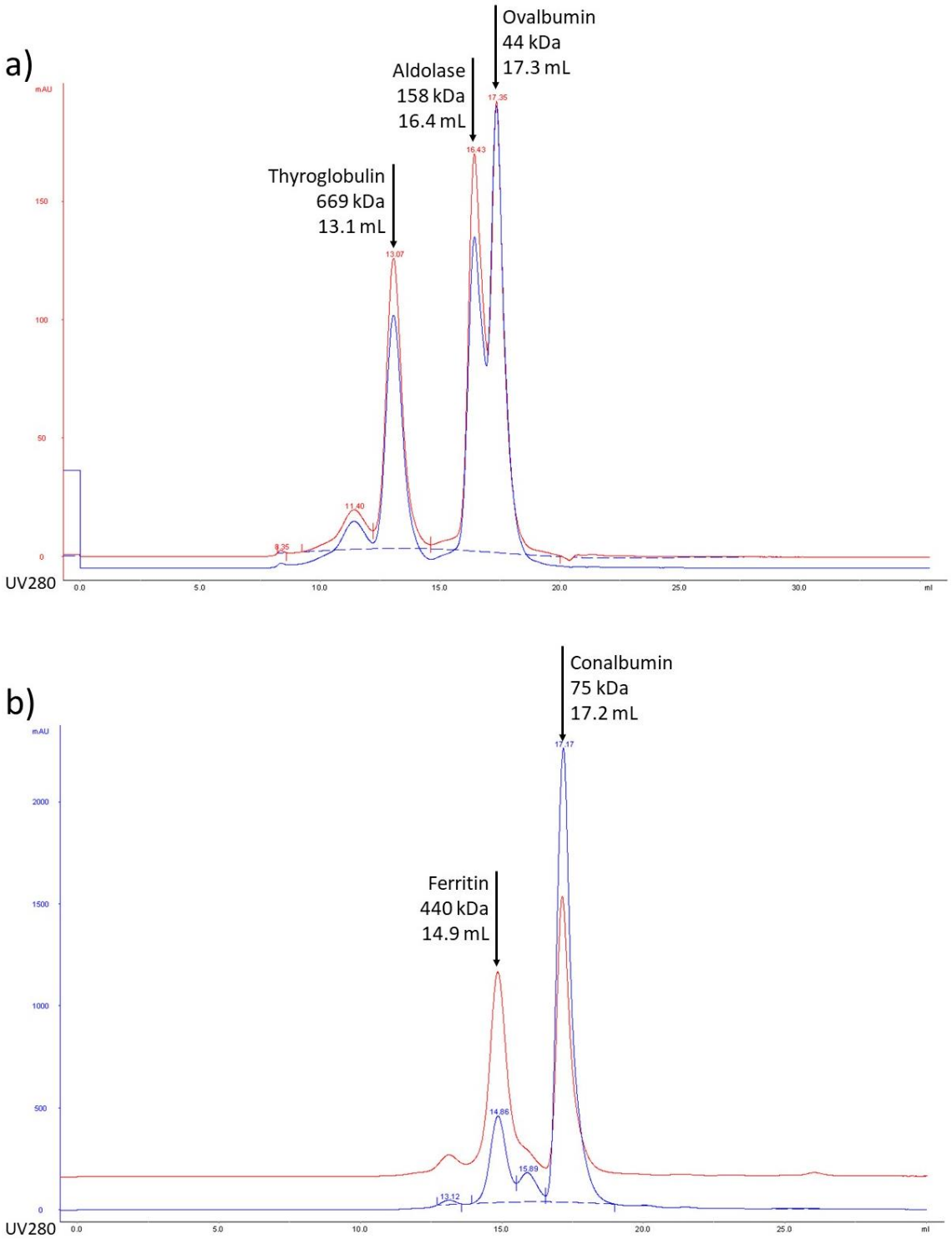

Figure 22 Size exclusion standards injected on Superose 6 Increase 10/300 column (a) thyroglobulin, aldolase, and ovalbumin standards; (b) ferritin and conalbumin standards

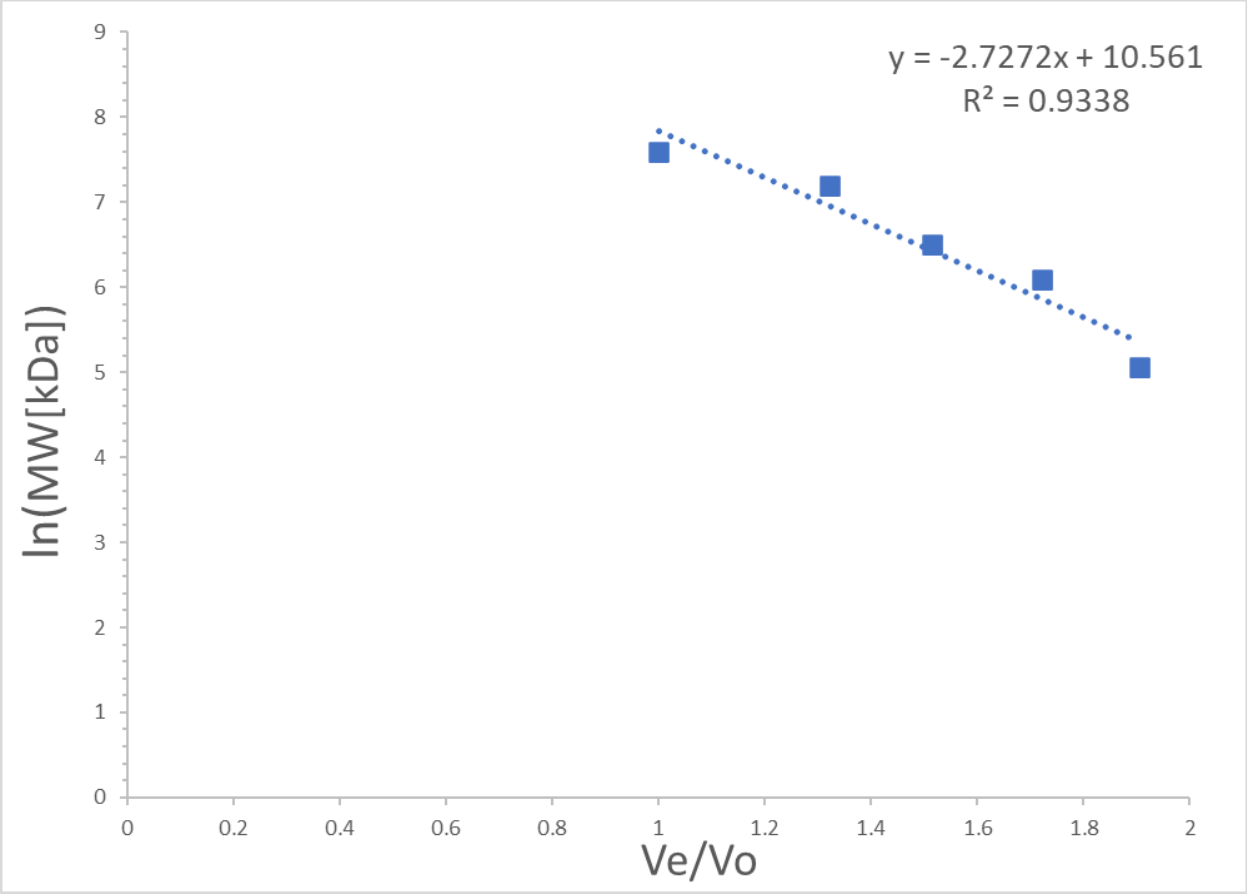

Figure 23 MW calibration curve for Superose 6 Increase 10/300

An S-2P IMAC elution sample was injected on the Superose 6 Increase 10/300 column and the A280 absorption curve can be viewed in ***Figure 24***. The asymmetric shape of the main peak at 12.16 mL retention volume could indicate different aggregated forms of the spike protein trimer are present in the sample. Using the calibration curve, all species eluted much earlier than the estimated retention volume, 14.0 mL, for a spike protein trimer about 426 kDa in size. The extrapolated MW sizes of the leading shoulders, 8.9- and 10.8-mL retention volume, are shown in ***Table 6*** and point to aggregated forms of the spike protein The rest of the chromatogram consists of protein impurities and/or degradation products with MWs less than 150 kDa; we

speculate that majority of the smaller MW species are spike degradation products since these have been eluted from IMAC.

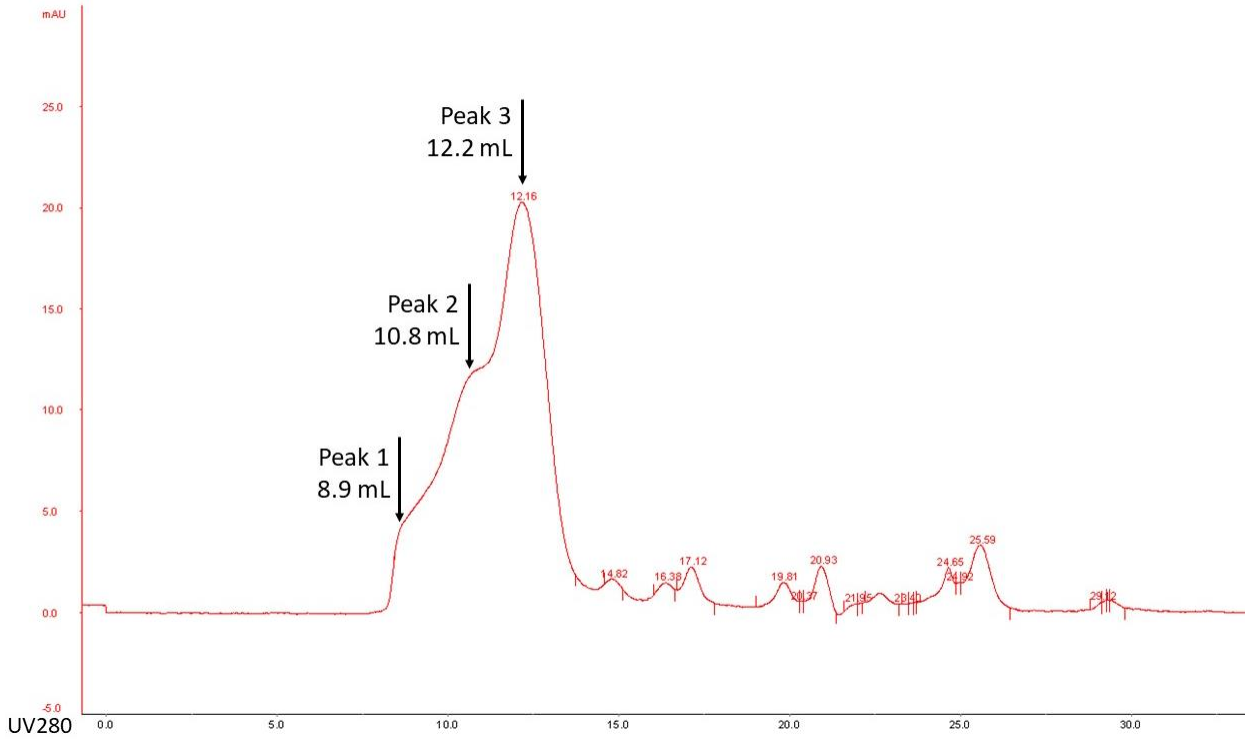

Figure 24 chromatogram of S-2P after IMAC on Superose 6 Increase 10/300

Table 6 Size estimates of S-2P peaks in Figure 24

Peak	Retention volume (mL)	Estimated MW (kDa)	Assumed aggregate
Peak 1	8.9	2347	~3 spike trimers
Peak 2	10.8	1247	~2 spike trimers
Peak 3	12.2	827	Spike trimer

Upon desalting of the IMAC S-2P elution pool by gel filtration column, the proportion of aggregated S-2P trimer increases. In ***Figure 25***, the middle peak now overwhelms the peak at 11.9 mL. Estimated MW are listed in ***Table 7*** There is a slight shift in retention volumes which is typical for unresolved peaks and shoulders due to change in MW distribution of the unresolved

aggregated species (trimeric and trimeric aggregate). It is believed that the 12.2 mL peak in ***Figure 24*** and 11.9 mL peak in ***Figure 25*** corresponds to the trimeric S-2P, while the remaining peaks in ***Figures 24*** and ***25*** belong to trimer aggregates. The smaller MW degradation products were removed through the course of the gel filtration column.

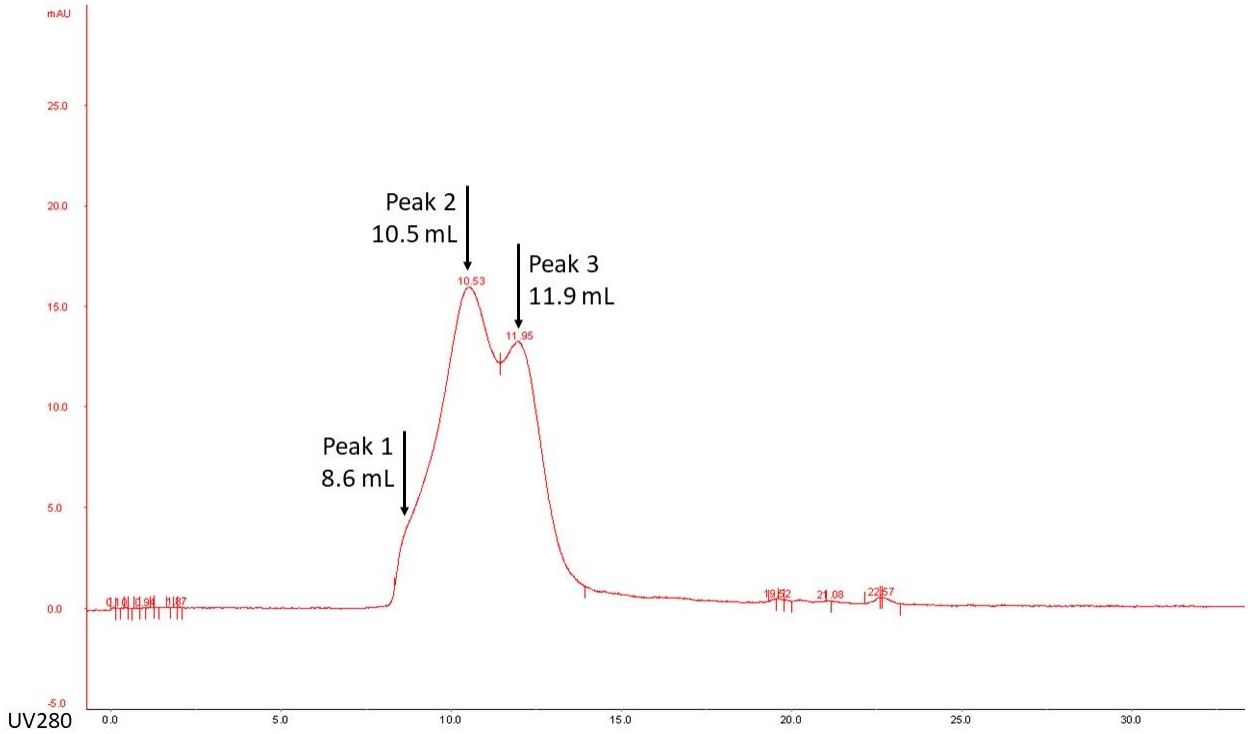

Figure 25 chromatogram of S-2P after imidazole removal on Superose 6 Increase 10/300

Table 7 Size estimates of S-2P peaks in Figure 25

Peak	**Retention volume (mL)**	**Estimated MW (kDa)**	**Assumed aggregate**
Peak 1	8.6	2548	~3 spike trimers
Peak 2	10.5	1384	~2 spike trimers
Peak 3	11.9	884	Spike trimer

The HexaPro spike protein variant also displayed similar aggregation tendencies throughout processing. Researchers were curious if nickel ions had leached from the nickel-

charged IMAC column and acted as nucleation points for agglomeration. It is important to note that StrepTactin affinity chromatography was utilized for this primary capture step of the HexaPro variant. The variation in retention time and number of peaks for the HexaPro samples could be due to isolation with a different affinity method using the TwinStrep-tag vs the His-tag. ***Figure 26*** shows two distinctly resolved peaks on size exclusion chromatography corresponding to aggregated forms of the spike protein variant in the elution pool after affinity chromatography. ***Table 8*** gives size estimates of these peaks. This finding is significant as it demonstrates the spike protein tendency towards aggregation in the absence of nickel ions.

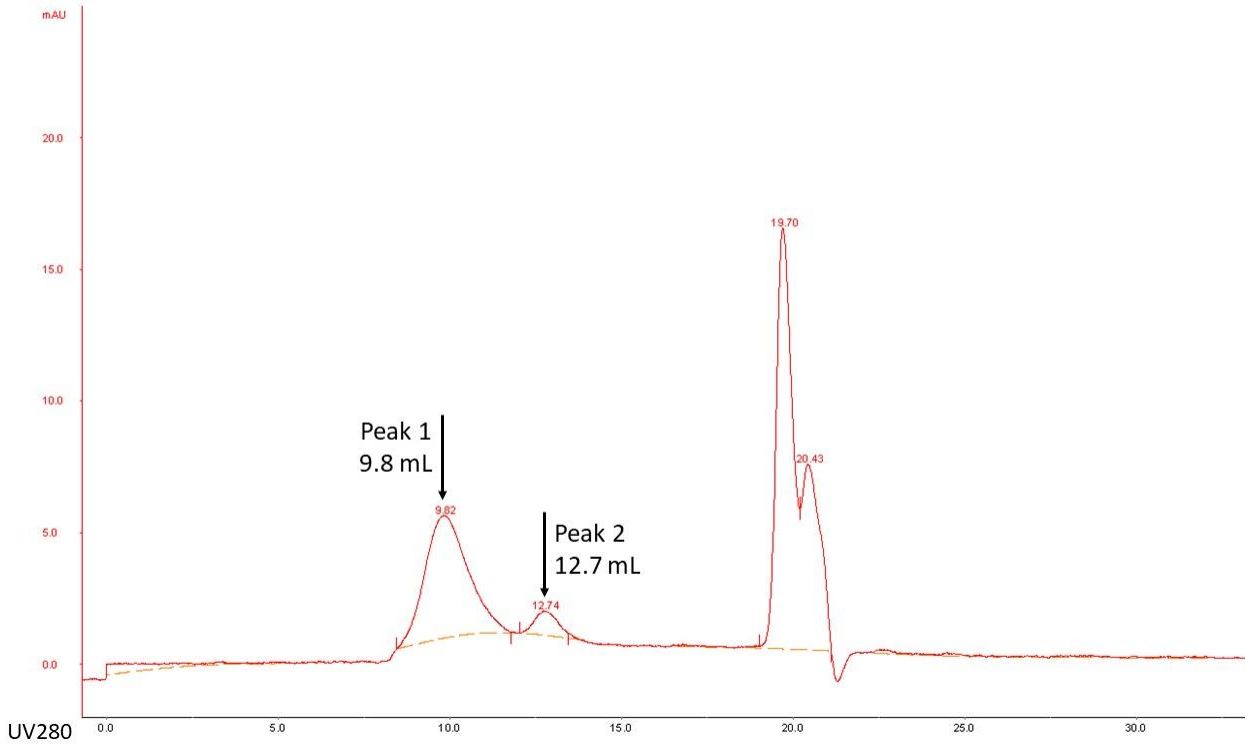

Figure 26 chromatogram of HexaPro after StrepTrap HT on Superose 6 Increase 10/300

Table 8 Size estimates of peaks in Figure 26

Peak	Retention volume (mL)	Estimated MW (kDa)	Assumed aggregate
Peak 1	9.8	1733	~3 spike trimers
Peak 2	12.7	688	Spike trimer

3.3.5 Effect of protease treatment on MW distribution of S-2P and HexaPro trimers

To determine the possible cause for induced aggregation/turbidity we examined the effect of tail removal. The results of Hsieh et al. [50] in ***Figure 18*** prompted us to consider the removal of the His- and Strep- tails and determine if the highly hydrophobic tail was one of the culprits for the observed turbidity and aggregation.

After protease treatment, the peak associated with large molecular weight aggregates of S-2P is no longer seen in ***Figure 27***. The single peak at 12.30 mL retention volume corresponds to the spike trimer. The retention volume of HexaPro spike proteins shifts following protease incubation; ***Figure 28*** indicates the cleaved sample runs as a smaller species through the column. Comparing ***Figure 26*** to ***Figure 28*** shows the shift in sizing. The small peaks at 19.7 and 20.4 mL retention volume correspond to the protease and the cleaved tags.

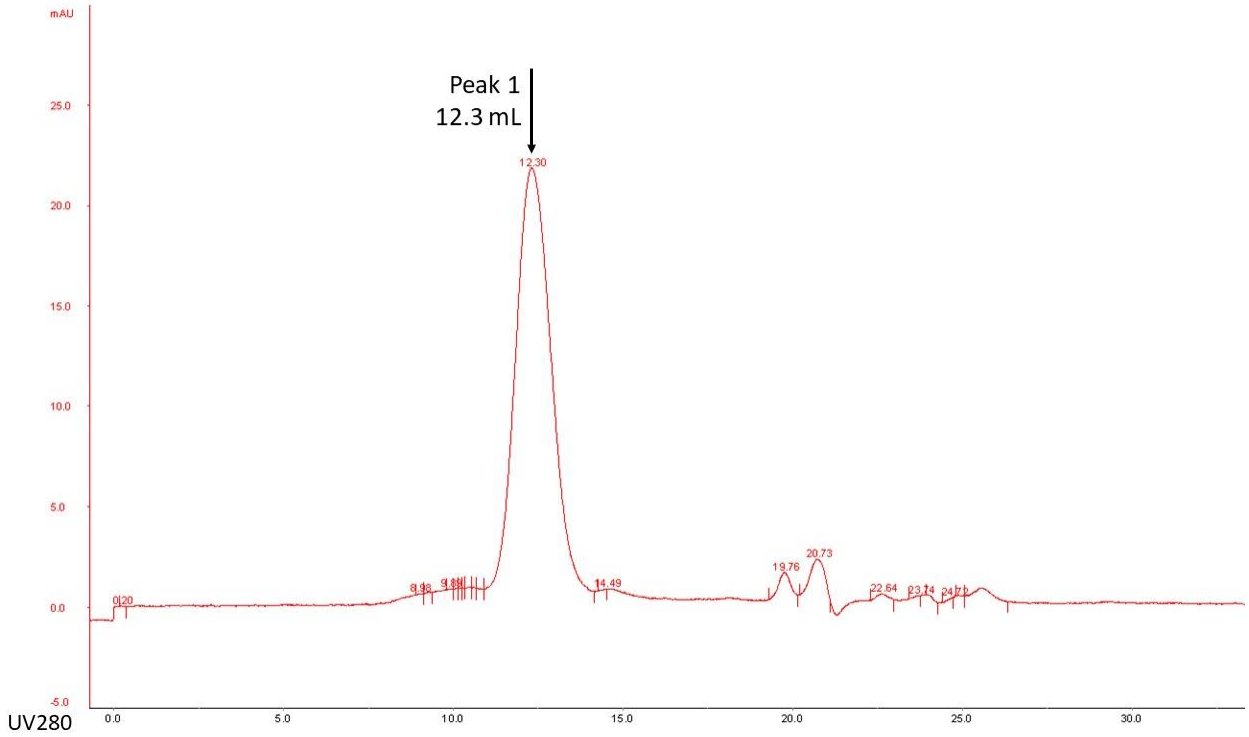

Figure 27 chromatogram of protease treated S-2P on Superose 6 Increase 10/300

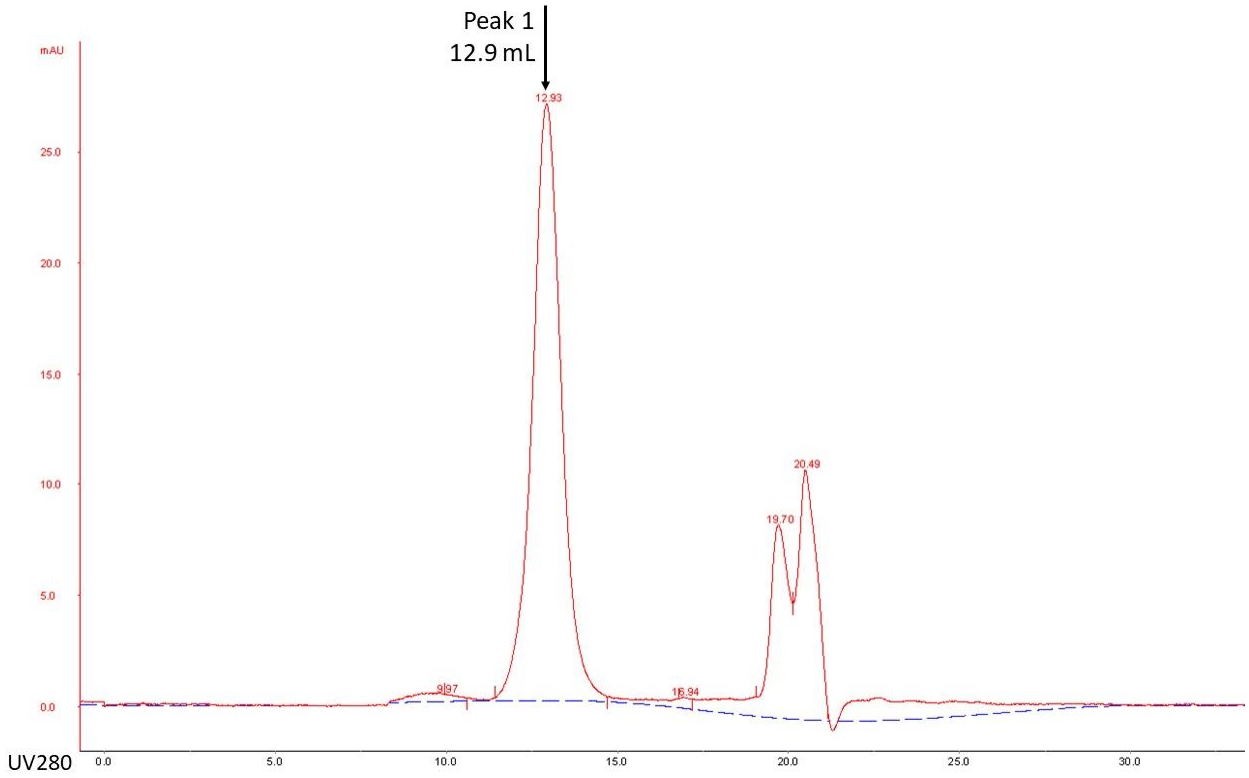

Figure 28 chromatogram of protease treated HexaPro on Superose 6 Increase 10/300 single main peak at 12.9 mL retention volume

3.4 Conclusions

In this study, Covid-19 spike protein variants were cultivated, purified, and assessed for quality after experiencing substantial increases in turbidity. When spike protein samples were analyzed by SEC, multiple unresolved peaks or one main peak with leading shoulders were observed. The retention volume of the early peaks corresponded to roughly double or triple the expected molecular weight estimates for the spike protein. Material from the IMAC EP, desalted EP, or TFF retentate all had these large species present in the sample - even visibly non-turbid material appeared to be in this aggregated form when run on SEC using HPLC.

When run on SEC, protease treated spike protein samples have a single, well resolved peak roughly corresponding to the size of a spike protein trimer. Thus, it is believed that the

hydrophobic nature of both the His-tag and Twin-Strep tags encouraged the tails to cluster together in an aqueous environment. The result appears to be aggregated spike protein trimers when run on SEC. While aggregation was present already, the shear experienced by the proteins during TFF greatly increased the amount of aggregation to a visible level.

3.5 Recommendations for future work

Future research in this area should include parallel processing of IMAC purified spike protein EP that 1) received protease treatment and 2) did not receive protease treatment. Then perform concentration and diafiltration on TFF as indicated in this study and compare protein quality on PAGE and SEC between the cleaved and uncleaved spike protein variants.

3.6 Acknowledgements

I would like to thank all the NCTM researchers for their time and expertise, assistance with experimentation and data collection, and allowing the use of their facility and equipment. I would like to thank the collaborators Dr. Jimmy Gollihar and Dr. Jason McLellan of the Army Futures Command Army Research Lab – South for providing cell culture stocks and expertise in processing design.

This work was also made possible by the Coronavirus Aid, Relief, and Economic Security (CARES) Act which allotted funding to the National Institute for Innovation in Manufacturing Biopharmaceuticals (NIIMBL); a public-private partnership sponsored by the National Institute of Standards and Technology (NIST) housed in the U.S. Department of Commerce; to support the project “Emergency Production of Covid-19 Spike Protein for

Therapeutic Antibodies and Diagnostics." Its contents are solely the responsibility of the authors and do not necessarily represent the official views of NIIMBL.

CHAPTER IV

CONCLUSIONS

This research looked at processing concerns for two different kinds of mammalian cell products: 1) mAb producing CHO cells and 2) Covid-19 spike protein producing HEK293 cells.

HCCS clarification filter flush buffers were tested for enhanced mAb recovery and impurity removal. It was found that performing a “blow-out” after filtration could recover an additional 10% of mAb from the preliminary experiments. The buffer conditions had no statistical impact on mAb recovery or HCP removal but had significant influence on dsDNA content. The high salt flush released DNA that had bound to the filter. For this reason, DI water is recommended as the chase buffer.

When Covid-19 spike protein variants were purified, turbidity was observed. These samples analyzed by SEC showed multiple unresolved peaks corresponding to much higher-than-expected molecular weight estimates for the spike protein. On the other hand, when protease treated spike protein samples were run on SEC, they showed a single peak corresponding to the size of a spike protein trimer. It is hypothesized that the aqueous environment encouraged clustering of the hydrophobic tails (his-tag and twin strep tag) effectively aggregating the spike trimers into much larger aggregates of 2 or more spike protein trimers. To corroborate this theory, parallel processing of cleaved and uncleaved spike protein variants should be assessed.

REFERENCES

1. Johnson, D., *Biotherapeutics: Challenges and Opportunities for Predictive Toxicology of Monoclonal Antibodies.* International Journal of Molecular Sciences, 2018. **19**(11): p. 3685.
2. Khan, S., et al., *Role of Recombinant DNA Technology to Improve Life.* International Journal of Genomics, 2016. **2016**: p. 1-14.
3. Rader, R.A. and E.S. Langer, *BioPharma Market: An Inside Look*, in *Biopharma Manufacturing Trends*. 2019. p. 4-11.
4. Sommerfeld, S. and J. Strube, *Challenges in biotechnology production—generic processes and process optimization for monoclonal antibodies.* Chemical Engineering and Processing: Process Intensification, 2005. **44**(10): p. 1123-1137.
5. Dumont, J., et al., *Human cell lines for biopharmaceutical manufacturing: history, status, and future perspectives.* Critical Reviews in Biotechnology, 2016. **36**(6): p. 1110-1122.
6. Zhang, W., et al., *Development an effective system to expression recombinant protein in E. coli via comparison and optimization of signal peptides: Expression of Pseudomonas fluorescens BJ-10 thermostable lipase as case study.* Microbial Cell Factories, 2018. **17**(1).
7. Jacob, E., A. Horovitz, and R. Unger, *Different mechanistic requirements for prokaryotic and eukaryotic chaperonins: a lattice study.* Bioinformatics, 2007. **23**(13): p. i240-i248.
8. Greene, E., et al., *Optimization of a transient antibody expression platform towards high titer and efficiency.* Biotechnology Journal, 2021. **16**(4): p. 2000251.

9. Wheelwright, S.M., *Designing Downstream Processes for Large–Scale Protein Purification.* Nature Biotechnology, 1987. **5**(8): p. 789-793.

10. Leser, E.W. and J.A. Asenjo, *Rational design of purification processes for recombinant proteins.* Journal of Chromatography B: Biomedical Sciences and Applications, 1992. **584**(1): p. 43-57.

11. Nfor, B.K., et al., *Rational and systematic protein purification process development: the next generation.* Trends in Biotechnology, 2009. **27**(12): p. 673-679.

12. Björkman, T., *Fig 1. Strategy for protein purification.*, digi-46737-original, Editor. 2022: https://www.cytivalifesciences.com/en/us/solutions/bioprocessing/knowledge-center/a-guide-to-polishing-chromatography.

13. Singh, N., et al., *Development of adsorptive hybrid filters to enable two-step purification of biologics.* mAbs, 2017. **9**(2): p. 350-364.

14. Shukla, A.A. and J. Thömmes, *Recent advances in large-scale production of monoclonal antibodies and related proteins.* Trends in Biotechnology, 2010. **28**(5): p. 253-261.

15. Butler, M. and A. Meneses-Acosta, *Recent advances in technology supporting biopharmaceutical production from mammalian cells.* Applied Microbiology and Biotechnology, 2012. **96**(4): p. 885-894.

16. Harrison, R.G., et al., *Bioseparations science and engineering*. 2015: Topics in Chemical Engineering.

17. Nejatishahidein, N., et al., *Scale-up issues for commercial depth filters in bioprocessing.* Biotechnology and Bioengineering, 2022. **119**(4): p. 1105-1114.

18. Shukla, A.A. and J.R. Kandula, *Harvest and Recovery of Monoclonal Antibodies from Large-Scale Mammalian Cell Culture.* Biopharm International, 2008. **21**(5): p. 34-36,38,40,42,44-45.

19. Liu, H.F., et al., *Recovery and purification process development for monoclonal antibody production.* mAbs, 2010. **2**(5): p. 480-499.

20. Felo, M., B. Christensen, and J. Higgins, *Process cost and facility considerations in the selection of primary cell culture clarification technology.* Biotechnology Progress, 2013. **29**(5): p. 1239-1245.

21. Yigzaw, Y., et al., *Exploitation of the Adsorptive Properties of Depth Filters for Host Cell Protein Removal during Monoclonal Antibody Purification.* Biotechnology Progress, 2006. **22**(1): p. 288-296.

22. Nguyen, H.C., et al., *Improved HCP Reduction Using a New, All-Synthetic Depth Filtration Media Within an Antibody Purification Process.* Biotechnology Journal, 2019. **14**(1): p. 1700771.

23. Chon, J.H., *Advances in the production and downstream processing of antibodies*, G. Zarbis-Papastoitsis, Editor. 2011, New Biotechnology. p. 458-463.

24. Buss, N.A.P.S., et al., *Monoclonal antibody therapeutics: history and future.* Current opinion in pharmacology, 2012. **12**(5): p. 615-622.

25. abcam, *Figure 2. Selective Binding of Nickel (Ni 2+) Chelated Resin to His-Tag Recombinant Protein.*, his---tag-image02, Editor. 2022: https://www.abcam.com/content/his-tag-protein-production-and-purification.

26. Bansal, R., S. Gupta, and A.S. Rathore, *Analytical Platform for Monitoring Aggregation of Monoclonal Antibody Therapeutics.* Pharmaceutical Research, 2019. **36**(11).

27. Arunkumar, A., et al., *Effect of channel-induced shear on biologics during ultrafiltration/diafiltration (UF/DF).* Journal of Membrane Science, 2016. **514**: p. 671-683.

28. Baek, Y. and A.L. Zydney, *Intermolecular interactions in highly concentrated formulations of recombinant therapeutic proteins.* Current Opinion in Biotechnology, 2018. **53**: p. 59-64.

29. Binabaji, E., et al., *Ultrafiltration of highly concentrated antibody solutions: Experiments and modeling for the effects of module and buffer conditions.* Biotechnology Progress, 2016. **32**(3): p. 692-701.

30. Den Engelsman, J., et al., *Strategies for the assessment of protein aggregates in pharmaceutical biotech product development.* Pharmaceutical research, 2011. **28**(4): p. 920-933.

31. Roberts, C.J., *Therapeutic protein aggregation: mechanisms, design, and control.* Trends in biotechnology, 2014. **32**(7): p. 372-380.

32. Jiskoot, W., et al., *Protein instability and immunogenicity: roadblocks to clinical application of injectable protein delivery systems for sustained release.* J Pharm Sci, 2012. **101**(3): p. 946-54.

33. Ghosh, S., et al., *Aggregation dynamics of charged peptides in water: Effect of salt concentration.* The Journal of Chemical Physics, 2019. **151**(7): p. 074901.

34. Dimitrov, D.S., *Therapeutic Proteins*, in *Methods in Molecular Biology*. 2012, Humana Press. p. 1-26.

35. Lalonde, M.-E. and Y. Durocher, *Therapeutic glycoprotein production in mammalian cells.* Journal of Biotechnology, 2017. **251**: p. 128-140.

36. Bracewell, D.G., R. Francis, and C.M. Smales, *The future of host cell protein (HCP) identification during process development and manufacturing linked to a risk-based management for their control.* Biotechnology and Bioengineering, 2015. **112**(9): p. 1727-1737.

37. Hutchinson, N., et al., *Shear stress analysis of mammalian cell suspensions for prediction of industrial centrifugation and its verification.* Biotechnology and Bioengineering, 2006. **95**(3): p. 483-491.

38. Iammarino, M., et al., *Impact of cell density and viability on primary clarification of mammalian cell broth: an analysis using disc-stack centrifugation and charged depth filtration.* BioProcess International, 2007. **5**(10): p. 38.

39. Shukla, A.A. and U. Gottschalk, *Single-use disposable technologies for biopharmaceutical manufacturing.* Trends in Biotechnology, 2013. **31**(3): p. 147-154.

40. Singh, N., et al., *Clarification of recombinant proteins from high cell density mammalian cell culture systems using new improved depth filters.* Biotechnology and Bioengineering, 2013. **110**(7): p. 1964-1972.

41. Kandula, S., et al., *Design of a filter train for precipitate removal in monoclonal antibody downstream processing.* Biotechnology and Applied Biochemistry, 2009. **54**(3): p. 149-155.

42. Shukla, A.A. and E. Suda, *HARVEST AND RECOVERY OF MONOCLONAL ANTIBODIES: CELL REMOVAL AND CLARIFICATION*, in *Process Scale Purification of Antibodies*. 2017. p. 55-79.

43. Nejatishahidein, N. and A.L. Zydney, *Depth filtration in bioprocessing — new opportunities for an old technology.* Current Opinion in Chemical Engineering, 2021. **34**: p. 100746.

44. Templeton, N., et al., *Peak antibody production is associated with increased oxidative metabolism in an industrially relevant fed-batch CHO cell culture.* Biotechnology and Bioengineering, 2013. **110**(7): p. 2013-2024.

45. Bibila, T.A. and D.K. Robinson, *In pursuit of the optimal fed-batch process for monoclonal antibody production.* Biotechnology Progress, 1995. **11**(1): p. 1-13.

46. Ejemel, M., et al., *A cross-reactive human IgA monoclonal antibody blocks SARS-CoV-2 spike-ACE2 interaction.* Nature Communications, 2020. **11**(1): p. 1-9.

47. Cucinotta, D. and M. Vanelli, *WHO Declares COVID-19 a Pandemic.* Acta Biomed, 2020. **91**(1): p. 157-160.

48. Li, F., *Structure, Function, and Evolution of Coronavirus Spike Proteins.* Annual Review of Virology, 2016. **3**(1): p. 237-261.

49. Esposito, D., et al., *Optimizing high-yield production of SARS-CoV-2 soluble spike trimers for serology assays.* Protein Expression and Purification, 2020. **174**: p. 105686.

50. Hsieh, C.-L., et al., *Structure-based design of prefusion-stabilized SARS-CoV-2 spikes.* Science, 2020. **369**(6510): p. 1501-1505.

51. Crank, M.C., et al., *A proof of concept for structure-based vaccine design targeting RSV in humans.* Science, 2019. **365**(6452): p. 505-509.

52. Sanders, R.W., et al., *A Next-Generation Cleaved, Soluble HIV-1 Env Trimer, BG505 SOSIP.664 gp140, Expresses Multiple Epitopes for Broadly Neutralizing but Not Non-Neutralizing Antibodies.* PLoS Pathogens, 2013. **9**(9): p. e1003618.

53. Pallesen, J., et al., *Immunogenicity and structures of a rationally designed prefusion MERS-CoV spike antigen.* Proceedings of the National Academy of Sciences, 2017. **114**(35): p. E7348-E7357.

54. Wrapp, D., et al., *Cryo-EM structure of the 2019-nCoV spike in the prefusion conformation.* Science, 2020. **367**(6483): p. 1260-1263.

55. Punde, N., et al., *Codon harmonization reduces amino acid misincorporation in bacterially expressed P. falciparum proteins and improves their immunogenicity.* AMB Express, 2019. **9**(1).